11

Control System Design

Yoonsu Nam
Department of Mechanical Engineering, Kangwon National University 192-1 Hyoja-2 dong, Chunchon, Kangwon 200-701 Korea

1. Introduction

A wind turbine control system is a complex and critical element in a wind turbine. It is responsible for the autonomous, reliable, and safe operation of the machine in all wind conditions. Two levels of control operations are required. One is supervisory control and the other is dynamic feedback control of blade pitch and generator torque for maximizing power production and minimizing mechanical loads on the wind turbine. The supervisory control system is one operating system of the wind turbine and has the following functions:

- operational state (stand-by, start-up, power production, shutdown) transition control
- control of subsystems (cooling, heating, hydraulics, etc.)
- diagnostics, alarm management
- data logging, statistics, post-processing
- user access (management), visualization.

A supervisory controller monitors the turbine and wind condition in order to decide when to start and shut down the wind turbine. Fig. 1 shows a schematic of the operational state transition logic which is implemented in supervisory control. A wind turbine operator can start and shut down turbine operation through a SCADA (supervisory control and data acquisition) system as shown in Fig. 1. The SCADA system can communicate with the supervisory controller in order to control and monitor the wind turbine.

The main topic of this chapter is the design of a control algorithm for the dynamic feedback controller which manages the blade pitch, the generator torque, and the yaw system. Most multi-MW wind turbines are equipped with variable speed and variable pitch (VSVP) technology (Leithead[b] & Connor, 2000; Bianchi et al., 2007; Muller et al., 2002; Boukhezzar et al., 2007). In the below rated wind speed conditions, the rotor speed varies with wind speed, while the pitch is fixed in order to maximize the energy capture from the wind. However, in the above rated wind speed conditions, the pitch is varied, while the rotor speed is fixed, in order for the machine to produce the rated power. All the analysis and design issues covered in this chapter for the dynamic feedback controller using VSVP technology target an upwind type horizontal axis multi-MW wind turbine having 3 blades. Yawing control is not dealt with here because of its simple on-off control logic. All the control algorithms covered in this chapter are based on classical control theory (Franklin et al., 2006; Dorf & Bishop, 2007).

This chapter is composed of 3 sections. Section 2 begins with a mathematical description of the wind, which is not only the source of energy but also a disturbing input to the wind

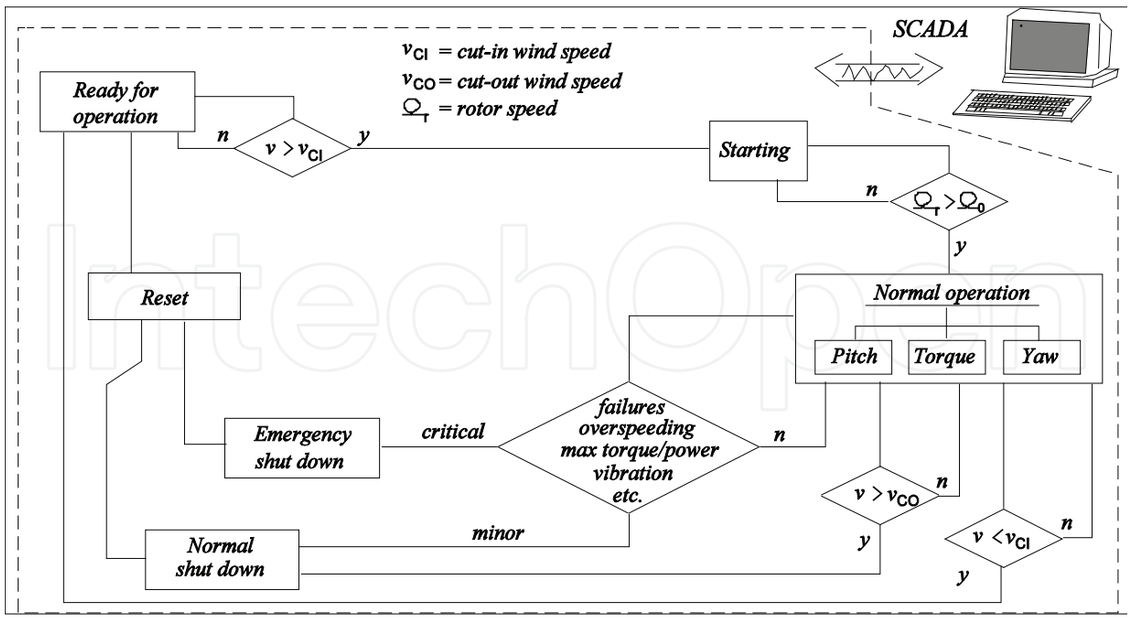

Fig. 1. Schematic of a wind turbine control system

turbine. The wind turbine control strategy and structure based on VSVP technology are explained. Simplified dynamic models of the pitch actuator and generator, which are elements of the wind turbine control system, are followed. Section 3 covers dynamic modeling and steady state characteristics of the wind turbine, based on a drive train model. Variables comprising rotor speed, wind speed, and pitch angle completely specify an operating condition of a wind turbine. How the dynamic characteristics vary with different operating conditions is analyzed in this section. Finally, Section 4 presents the main topic of this chapter, i.e. wind turbine control system design. It starts with the control system design requirements which are determined from the wind characteristics and the aeroelastic properties of the wind turbine structure. A methodology on how to set PI controller gains is introduced, considering gain scheduling and the integrator anti-windup problem. The section includes a feedforward pitch control system design using a wind speed estimator to enhance the performance of the output power regulation. This section concludes with the introduction of individual pitch control for mechanical load alleviation of the blades.

2. Wind turbine control system

2.1 Wind

Wind is highly variable. To accurately predict the wind ahead of time is almost impossible. Statistical measures such as mean wind speed and turbulence intensity are frequently used. Turbulence intensity is given by

$$I = \frac{\sigma}{\overline{v}} \tag{1}$$

where σ is the standard deviation of the wind speed and $\overline{v}$ is the mean wind speed, usually defined for 10 minutes of wind data. Fig. 2 shows two different winds, even though these have the same mean wind speed and turbulence intensity. One further statistical property,

i.e. autocorrelation, is necessary to discern the wind more specifically. The autocorrelation is defined as

$$\phi_{xx}(\tau) = E\{x(t)x(t+\tau)\} = \lim_{T\to\infty}\left\{\frac{1}{2T}\int_{-T}^{T} x(t)x(t+\tau)dt\right\} \tag{2}$$

where $x(t)$ is a de-trended time series. Therefore, $\varphi_{xx}(0)=\sigma_x^2$. As signal frequency increases and time-lag τ gets larger, the autocorrelation becomes smaller. The power spectral density, which is the Fourier transform of the autocorrelation, is defined as

$$\Phi_{xx}(\omega) = \int_{-\infty}^{\infty} \phi_{xx}(\tau)e^{-j\omega\tau}d\tau \ . \tag{3}$$

A sample of the autocorrelation and power spectral density for two different time series is shown in Fig. 3.

Van der Hoven observed at Brookhaven, New York, in 1957 that there were distinct periodicities in wind, as shown in Fig. 4 (van der Hoven, 1957). Three peaks, namely synoptic, diurnal, and turbulent peaks, are clear in this plot. On a short time scale of less than 2 hours, turbulent wind has most energy in the wind spectrum. The power spectral density of turbulent wind can be modeled as

$$\Phi_{vv}(\omega) = \frac{4\sigma_u^2 L_u / \overline{v}}{\left(1+70.8\left(\omega L_u / (2\pi\overline{v})\right)^2\right)^{5/6}} \tag{4}$$

where σ_u is the standard deviation for a turbulent wind and L_u is the length scale (Burton et al., 2001). The length scale is a site-specific parameter and depends on the surface roughness a and height z. It is given by

$$L_u = 280(z / z_i)^{0.35} \ . \tag{5}$$

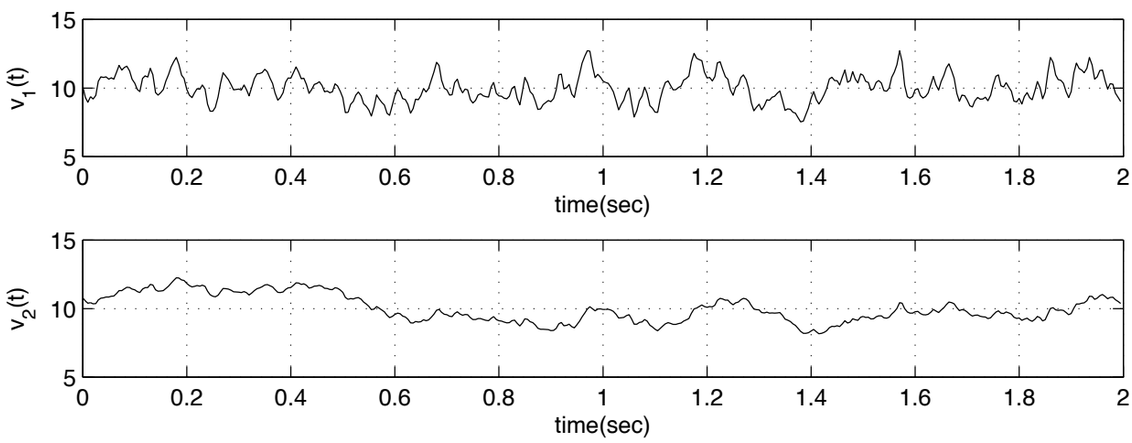

Fig. 2. Two different winds with the same mean wind speed and turbulence intensity

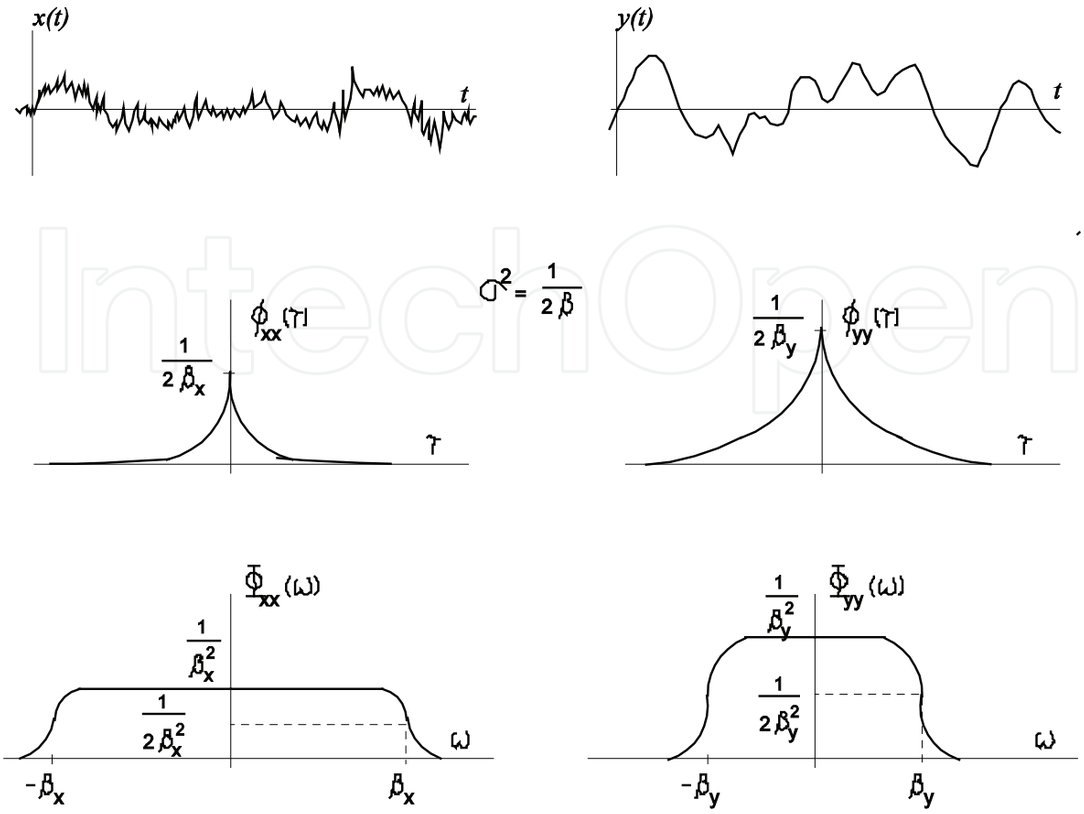

Fig. 3. Autocorrelation and power spectral density

Some representative values of a are given in Table 1 with the value of z_i. The turbulence becomes isotropic for the condition of $L_u \geq 280$ m at an altitude of $z > z_i$. The above expression of Eq. (4) is known as the von Karman spectrum in the longitudinal direction. The von Karman expressions in the lateral and vertical directions can be found in the literature (Burton et al., 2001).

2.2 Control system strategies and structure

The mechanical power of an air mass which has a flow rate of dm/dt with a constant speed of v is given by

$$P = \frac{d}{dt}(E) = \frac{d}{dt}\left(\frac{1}{2}mv^2\right) = \frac{1}{2}\frac{dm}{dt}v^2 = \frac{1}{2}\rho A v^3 \tag{6}$$

where ρ is the air density and A is the cross sectional area of the air mass. Only a portion of the wind power given by Eq. (6) is converted to electric power by a wind turbine. The efficiency of the power conversion by a wind turbine depends on the aerodynamic design and operational status of the wind turbine. Usually, the power generated by the wind turbine is represented by

$$P = C_P\left(\frac{1}{2}\rho A v^3\right) \tag{7}$$

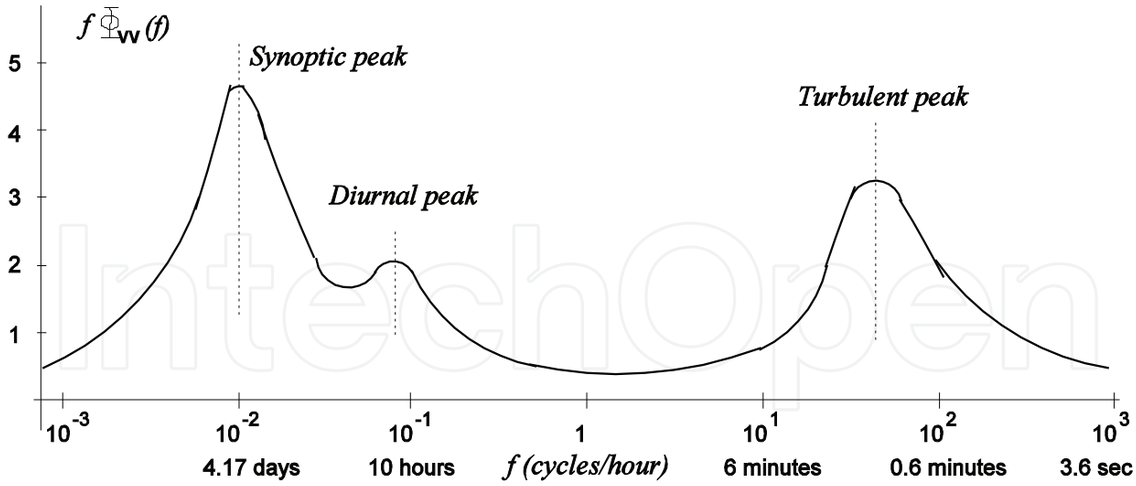

Fig. 4. van der Hoven wind spectrum

Type of terrain	Roughness length α (m)	z_i=1000$a^{0.18}$ (m)
Cities, forests	0.7	937.8
Suburbs, wooded countryside	0.3	805.2
Villages, countryside with tress and hedges	0.1	660.7
Open farmland, few trees and buildings	0.03	532.0
Flat grassy plains	0.01	436.5
Flat desert, rough sea	0.001	288.4

Table 1. Surface roughness (Burton et al., 2001)

where Cp represents the efficiency of wind power conversion and is called the power coefficient. The ideal maximum value of Cp is 16/27= 0.593, which is known as the Betz limit (Manwell et al., 2009).

As shown in Fig. 5, the power coefficient, Cp is a function of pitch angle β and tip speed ratio λ which is defined as

$$\lambda = \frac{R\Omega_r}{v} \tag{8}$$

where R is the rotor radius and Ω_r is the rotor speed of the wind turbine. Fig. 5 is a sample plot of Cp for a multi-MW wind turbine. The curve with dots shows the variation of Cp with λ for a fixed pitch angle of β_0. As the pitch angle is away from β_0, the value of Cp becomes smaller. Therefore, Cp has the maximum with the condition of $\lambda=\lambda_0$ and $\beta=\beta_0$. In order for a wind turbine to extract the maximum energy from the wind, the wind turbine should be operated with the max-Cp condition. That is, the wind turbine should be controlled to maintain the fixed tip speed ratio of $\lambda=\lambda_0$ with the fixed pitch of $\beta=\beta_0$ in spite of varying wind speed. Referring to Eq. (8), there ought to be a proportional relationship between the wind speed v and the rotor speed Ω_r to keep the tip speed ratio at constant value of λ_0.

Fig. 6 represents a power curve which consists of three operational regions. Region I is max-Cp, Region II is a transition, and Region III is a power regulation region.

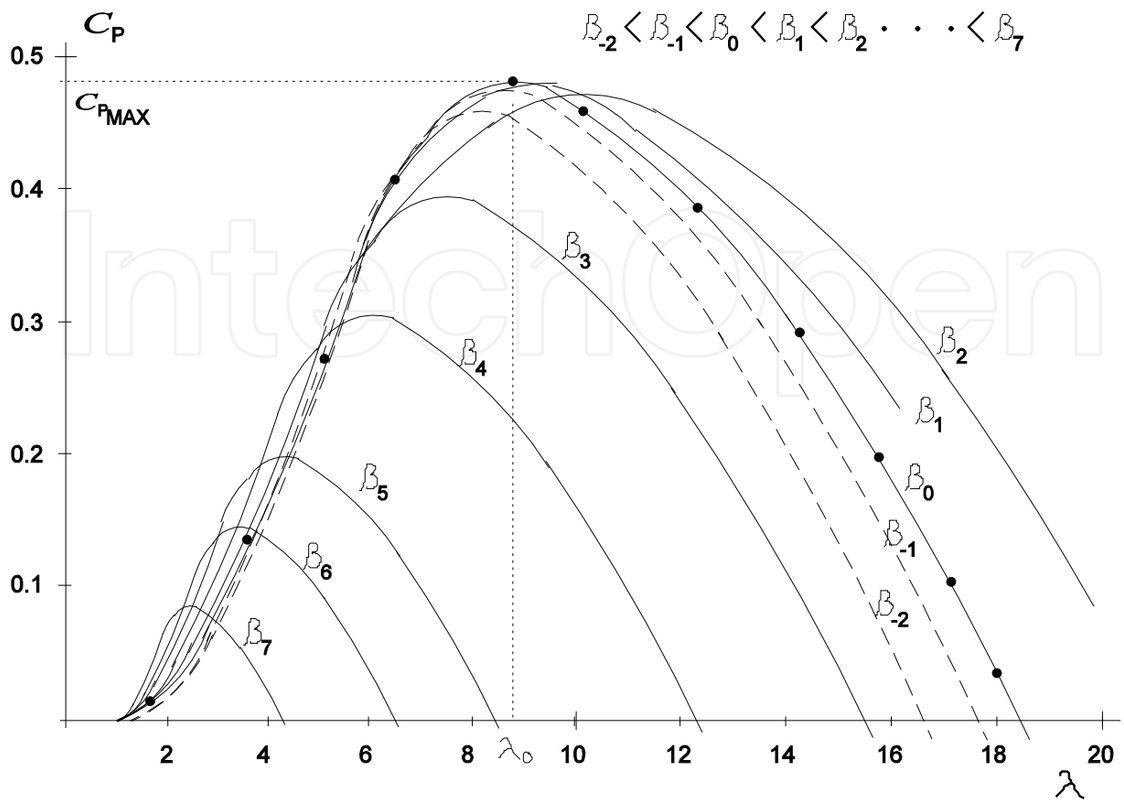

Fig. 5. Sample plot of Cp as a function of λ and β

- Region I: The wind turbine is operated in max-Cp. The blade pitch angle is fixed at β_0 and the rotor speed is varied so as to maintain the tip speed ratio constant (λ_0). Therefore, the rotor speed is changed so as to be proportional to the wind speed by controlling the generator reaction torque. In the max-Cp region, the generator torque control is active only, while the blade pitch is fixed at β_0.
- Region II: This is a transition region between the other two regions, that is the max-Cp (Region II) and power regulation region (Region III). Several requirements, such as a smooth transition between the two regions, a blade-tip noise limit, minimal output power fluctuations, etc., are important in defining control strategies for this region.
- Region III: This is the above rated wind speed region, where wind turbine power is regulated at the rated power. Therefore, rotor speed and generator reaction torque are maintained at their rated values. In this region, the value of Cp has to be controlled so as to be inversely proportional to v^3 to regulate the output power to the rated value. This is easily found by noting Eq. (1). In this region, the blade pitch control plays a major role in this task.

A control system structure for a wind turbine is shown schematically in Fig. 7. There are two feedback loops. One is the pitch angle control loop and the other is the generator torque control loop. Below the rated wind speed region, i.e. in Regions I and II, the blade pitch angle is fixed at β_0 and the generator torque is controlled by a prescheduled look-up table (see Section 3.2). The most common types of generator for a multi-MW wind turbine are a doubly fed induction generator (DFIG) (Soter & Wegerer, 2007) and a permanent magnet

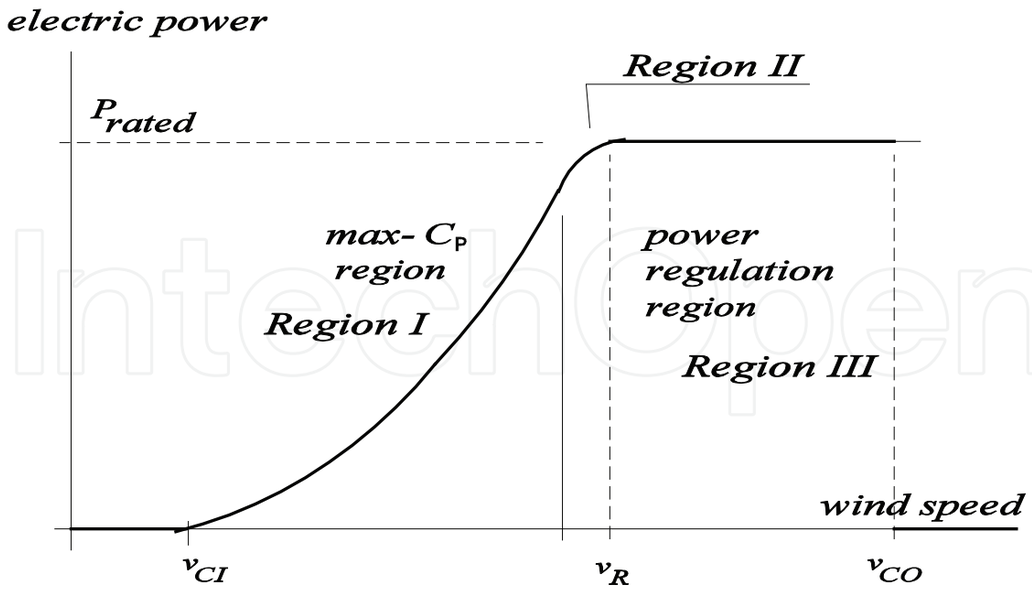

Fig. 6. Power curve

synchronous generator (PMSG) (Haque et al., 2010). These electric machines are complicated mechanical and electric devices including AC-DC-AC power converters. For the purposes of control system design, however, it is suffiicient to use a simple model of generator dynamics:

$$\frac{T_g(s)}{T_g^C(s)} = \frac{\omega_{ng}^2}{s^2 + 2\zeta_{ng}\omega_{ng}s + \omega_{ng}^2} \tag{9}$$

where $T_g{}^C$ is a generator torque command, ω_{ng} (~ 40 r/s) is a natural frequency of the generator dynamics and ζ_{ng} (~ 0.7) is a damping ratio (van der Hooft et al., 2003). Blade pitch angle is actuated by an electric motor or hydraulic actuator which can be modeled as

$$\frac{\beta(s)}{\beta^C(s)} = \frac{1}{1 + \tau_p s} \tag{10}$$

where β^C is a pitch angle demand and τ_p (~ 0.04 r/s) is a time constant of the pitch actuator. It is necessary and important for a realistic simulation to include saturation in actuator travel and its rate as depicted in Fig. 8 (Bianchi et al., 2007). In general, the pitch ranges from -3° to 90° and a maximum pitch rates of ±8°/s are typical values for a multi-MW wind turbine.

Power curve tracking and mechanical load alleviation are two main objectives of a wind turbine control system. For a turbulent wind, the wind turbine control system should not only control generation of electric power as specified in the power curve but also maintain structural loads of blades, drive train, and tower as small as possible. In the below rated wind speed region (max-Cp region), the generator torque control should be fast enough to follow the variation of turbulent wind. Generally, this requirement is not an issue because the electric system is much faster than the fluctuation of the turbulent wind. In the above rated wind speed region (power regulation region), the rotor speed should be maintained at

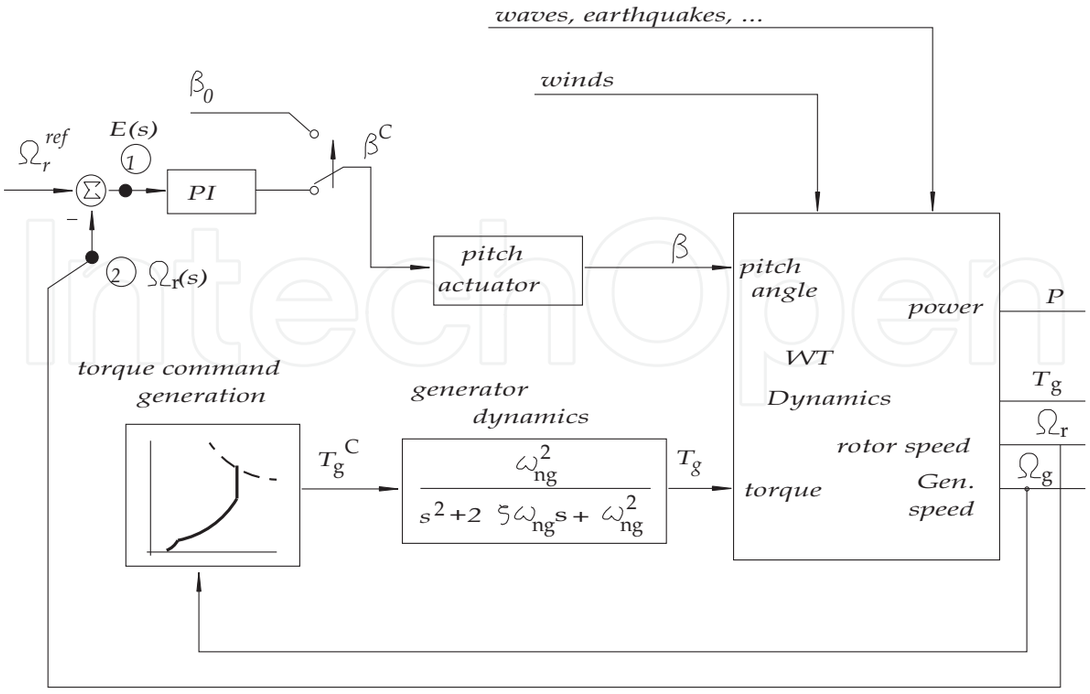

Fig. 7. Wind turbine control system structure

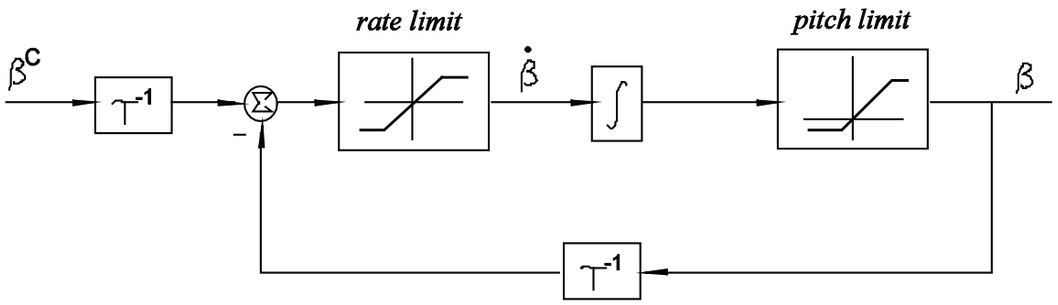

Fig. 8. Pitch actuator model

its rated speed by the blade pitch control, irrespective of wind speed fluctuation. The design of pitch control loop affects the mechanical loads of blades and tower as well as the performance of the wind turbine. Combined control of torque and pitch or the application of feedforward control (see Section 4.3) is a promising alternative for enhancing the power regulation performance. The alleviation of mechanical loads by the individual blade pitch control is discussed in Section 4.4.

3. Dynamic model and steady state operation

3.1 Drive train model and generator torque scheduling

A wind turbine is a complicated mechanical structure which consists of rotating blades, shafts, gearbox, electric machine, i.e. generator, and tower. Sophisticated design codes are necessary for predicting a wind turbine's performance and structural responses in a turbulent wind field. However, the simple drive train model of Fig. 9 is sufficient for control

system design (Leithead[a] & Connor, 2000). The parameters referred to in Fig. 9 are summarized in Table 2. The aerodynamic torque developed by the rotor blades can be obtained using Eq. (7) and Eq. (8) as follows

$$T_a = \frac{P}{\Omega_r} = \frac{1}{2}\rho\pi R^2 \frac{C_P(\lambda,\beta)}{\Omega_r} v^3 = \frac{1}{2}\rho\pi R^3 \frac{C_P(\lambda,\beta)}{\lambda} v^2 = \frac{1}{2}\rho\pi R^3 C_Q(\lambda,\beta) v^2 \tag{11}$$

where $C_Q = C_p/\lambda$ is the torque constant. The torque of Eq. (11) is counteracted by the generator torque. Therefore, the governing equations of motion for a drive train model are

$$\begin{aligned} J_r \frac{d\Omega_r}{dt} &= T_a - k_S(\theta_r - \frac{1}{N}\theta_g) - c_S(\Omega_r - \frac{1}{N}\Omega_g) - B_r\Omega_r \\ J_g \frac{d\Omega_g}{dt} &= \frac{k_S}{N}(\theta_r - \frac{1}{N}\theta_g) + \frac{c_S}{N}(\Omega_r - \frac{1}{N}\Omega_g) - B_g\Omega_g - T_g \end{aligned} \tag{12}$$

It is useful to understand the physical meaning of Fig. 10 which shows the relationship between rotor speed (Ω_r) and torque on a high speed shaft ($(T_a)_{HSS}$). The several mountain-shaped curves in this figure represent the aerodynamic torque on a high speed shaft for different wind speeds and rotor speeds at a fixed pitch β_o. These are easily calculated using Eq. (11) and power coefficient data from Fig. 5 for any specific wind turbine. On this plot, the max-Cp operational condition is shown as a dashed line, which satisfies the quadratic relation:

$$\begin{aligned} (T_a)_{HSS} &= \frac{1}{2N}\rho\pi R^3 \left(\frac{C_{P\max}}{\lambda_o}\right) v^2 = \frac{1}{2N}\rho\pi R^3 \left(\frac{C_{P\max}}{\lambda_o}\right)\left(\frac{\Omega_r R}{\lambda_o}\right)^2 \\ &= \frac{1}{2N}\rho\pi R^5 \frac{C_{P\max}}{\lambda_o^3}(\Omega_r)^2 = k_{op}\Omega_r^2 \end{aligned} \tag{13}$$

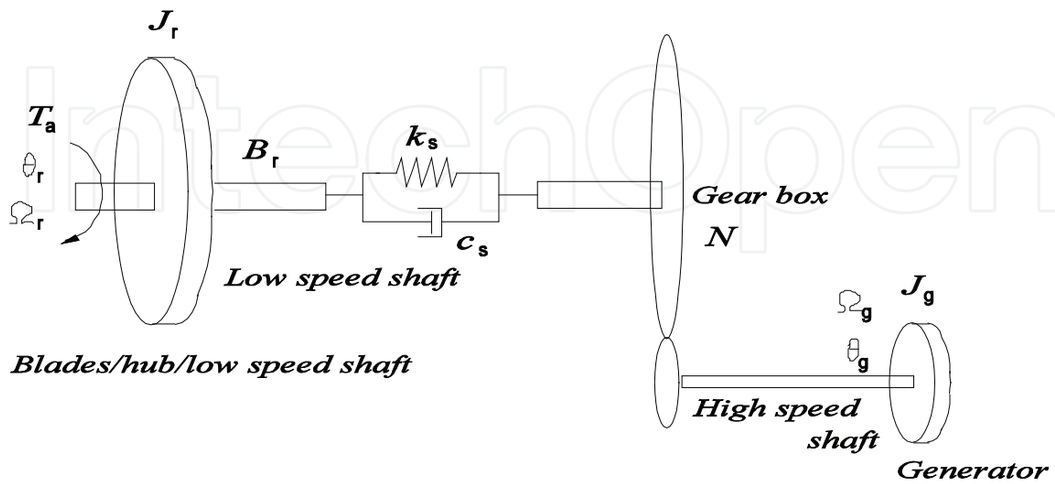

Fig. 9. Drive train model

Symbol	Description	unit
J_r	Inertia of three blades, hub and low speed shaft	Kgm^2
J_g	Inertia of generator	Kgm^2
B_r	Damping of low speed shaft	Nm/s
B_g	Damping of high speed shaft	Nm/s
k_s	Torsional stiffness of drive train axis	N
c_s	Torsional damping of drive train axis	Nm/s
N	Gear ratio	-
T_g	Generator reaction torque	Nm
Ω_g	Generator speed	r/s

Table 2. Parameters for the drive train model of Fig. 9

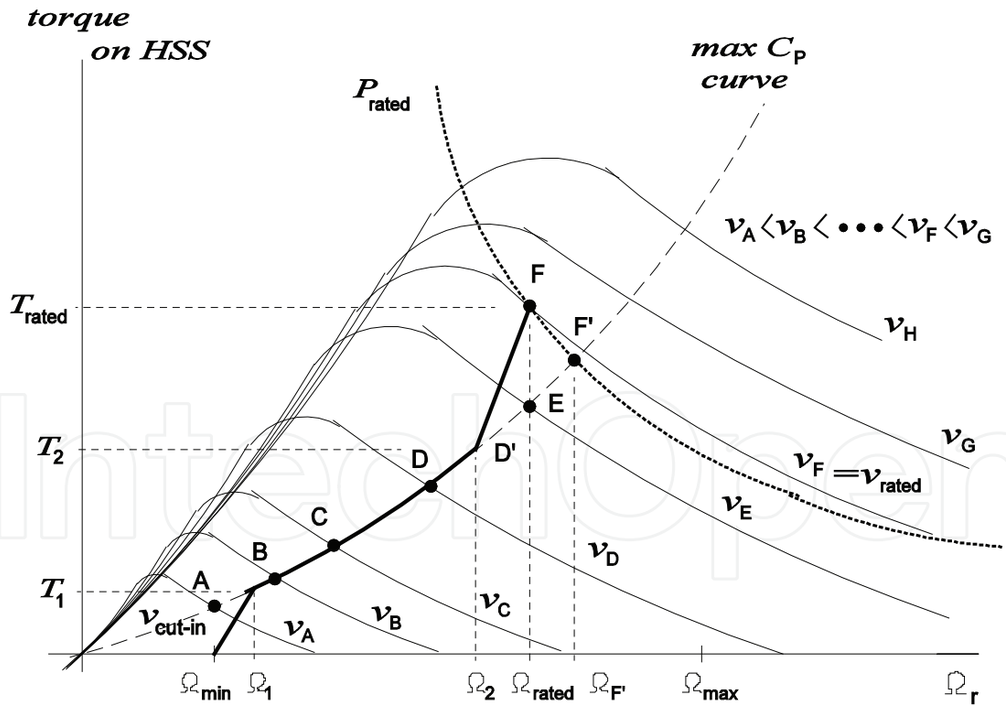

Fig. 10. Characteristic chart for torque on a high speed shaft and rotor speed

In the below rated wind speed region, a wind turbine is to be operated with the max-Cp condition to extract maximum energy from the wind. This means that the wind turbine should be operated at the point B for a steady wind speed v_B, the point C for a wind speed v_C, and so on in Fig. 10. For steady state operation, the aerodynamic torque of Eq. (13) should be counteracted by the generator reaction torque plus the mechanical losses from viscous friction, i.e. $B_r\Omega_r/N$ and $B_g\Omega_g$. Considering only the maximum energy capture, a torque schedule of A-B-C-D-E-F′ for a variable rotor speed is the optimal. However, the rated rotor speed might not be allowed to be as large as Ω_F′ because of the noise problem. If the tip speed ($R\Omega_r$) of a rotor is over around 75 m/s (Leloudas et al., 2007), then noise from the rotor blades could be critical for on-shore operation. Therefore, as the size of a wind turbine becomes larger, the rated rotor speed becomes smaller. Because of this constraint, the toque schedule for most multi-MW wind turbines has the shape of either A-B-C-D-E-F or A-B-C-D′-F. Wind turbines using a permanent magnet synchronous generator (PMSG) often have the torque schedule of A-B-C-D-E-F. In this case, the generator torque control of Fig. 7 using a look-up table is not appropriate because of the vertical section E-F. A PI controller with the max-Cp curve as the lower limit can be applied (Bossanyi, 2000).

3.2 Aerodynamic nonlinearity and stability

The nonlinearity of a drive train model comes from the aerodynamic torque of Eq. (11), which is a nonlinear function of three variables, (Ω_r, v, β). A single set of these variables defines a steady state operating condition of a wind turbine. The aerodynamic torque can be linearized for an operating condition of (Ω_{ro}, v_o, β_o) as follows:

$$\begin{aligned} T_a &= \frac{1}{2}\rho\pi R^3 C_Q(\lambda,\beta)v^2 = T_a(\Omega_r, v, \beta) \\ &\simeq T_a(\Omega_{r0}, v_0, \beta_0) + \left(\left.\frac{\partial T_a}{\partial \Omega_r}\right|_{(\Omega_{r0}, v_0, \beta_0)}\right)\delta\Omega_r + \left(\left.\frac{\partial T_a}{\partial v}\right|_{(\Omega_{r0}, v_0, \beta_0)}\right)\delta v + \left(\left.\frac{\partial T_a}{\partial \beta}\right|_{(\Omega_{r0}, v_0, \beta_0)}\right)\delta\beta \\ &= T_a(\Omega_{r0}, v_0, \beta_0) + B_\Omega\delta\Omega_r + B_v\delta v + k_\beta\delta\beta \end{aligned} \tag{14}$$

where $\delta\Omega_r = \Omega_r - \Omega_{ro}$, $\delta v = v - v_o$, $\delta\beta = \beta - \beta_o$.

Note that the sign of B_Ω is related with the stability of the wind turbine. The operating condition of (Ω_{ro}, v_o, β_o) where the B_Ω value is positive is unstable. This is clear on substituting the linearized aerodynamic torque of Eq. (14) into Eq. (12). Therefore, if a wind turbine is operating on the left side hill (positive slope, i.e. positive B_Ω region, which is also known as the stall region) of the mountain-shaped curve of Fig. 10, this means that the wind turbine is naturally (open loop) unstable. The coefficient B_v denotes just the gain of aerodynamic torque for a wind speed increase. The coefficient k_β represents the effectiveness of pitching to the aerodynamic torque. Fig. 11 shows a sample plot of these three coefficients as a function of wind speed for a multi-MW wind turbine. This plot is easily obtained using a linearizing tool, Matlab/Simulink© with Eq. (11). The line marked with 'x' shows B_Ω variation with wind speed in Nm/rpm. B_v data are shown with the symbol '+' in Nm/(m/s). The effectiveness of pitch angle on aerodynamic torque, i.e. k_β, is represented by the line with '◊' in Nm/deg. The values of k_β are zero in the low wind speed region, which means that the wind turbine is operating at the top of the Cp-curve, i.e. max-Cp (see Fig. 5). It gradually becomes negative because a blade pitching to feathering position decreases the aerodynamic torque. Note that the magnitudes of k_β in the rated wind speed region (12 m/s)

are relatively small compared to those at high wind speed. Because of this property, gain scheduling of the pitch loop controller is required (see Section 4.2).

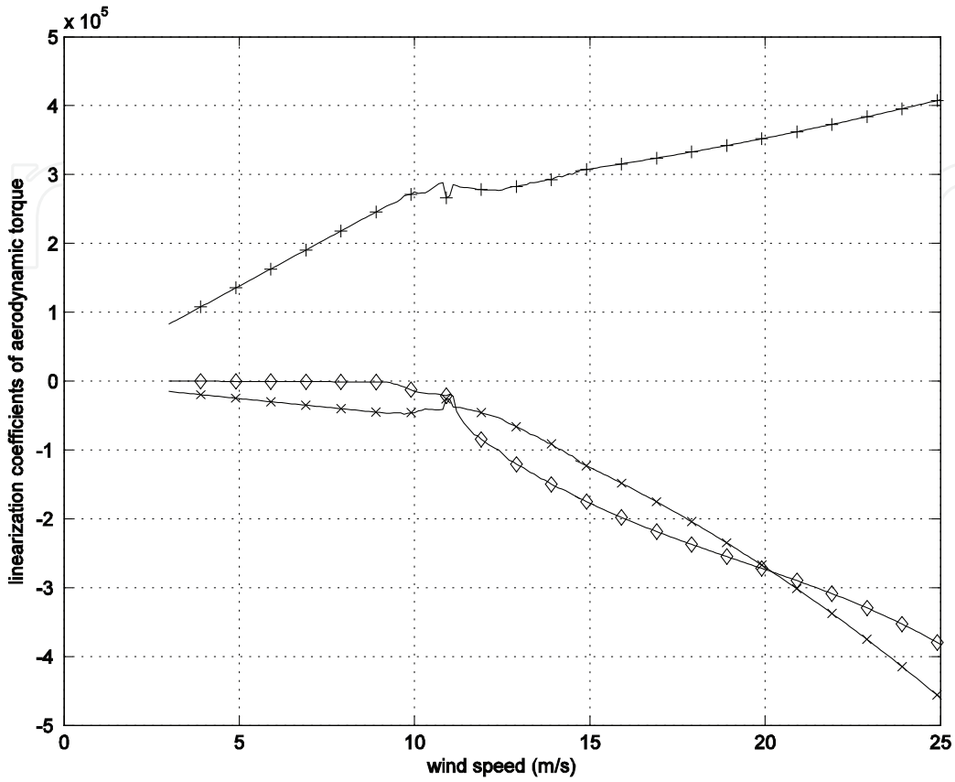

Fig. 11. Variation of B_Ω , B_v , and k_β with steady wind speeds for a multi-MW WT

3.3 Steady state operation

For a steady wind speed, a wind turbine should also be in steady state operation, i.e. with constant rotor speed and pitch angle. Therefore, a set of three variables, (Ω_r, v, β) defines a steady state operation condition of a wind turbine. How to determine these sets of variables is the topic of this section. In steady state operation, the dynamic equations of motion of Eq. (12) are combined to a nonlinear algebraic equation:

$$\frac{T_a}{N} - \frac{B_r \Omega_r}{N} - B_g \Omega_g - T_g = \frac{1}{2N} \rho \pi R^3 C_Q(\lambda, \beta) v^2 - \frac{B_r \Omega_r}{N} - N B_g \Omega_r - T_g = 0 \,. \tag{15}$$

Assuming that generator torque scheduling is completed as explained in Section 3.1 (see Fig. 10), generator torque T_g would be a function of rotor speed Ω_r. Therefore, a set of three variables, (Ω_r, v, β) constitutes the above nonlinear equation. To find one set of variables, (Ω_r, v, β) for a given wind speed v, one further relationship between these variables is needed, apart from Eq. (15). Fortunately, depending on the wind speed region, either pitch angle or rotor speed is fixed as explained in Section 2.2.

In the below rated wind speed region, blade pitch angle is fixed at β_0. Therefore, only one variable, which is the rotor speed, is unknown and can be determined by Eq. (15). However, an analytic solution is not possible, because the equation includes terms having numeric

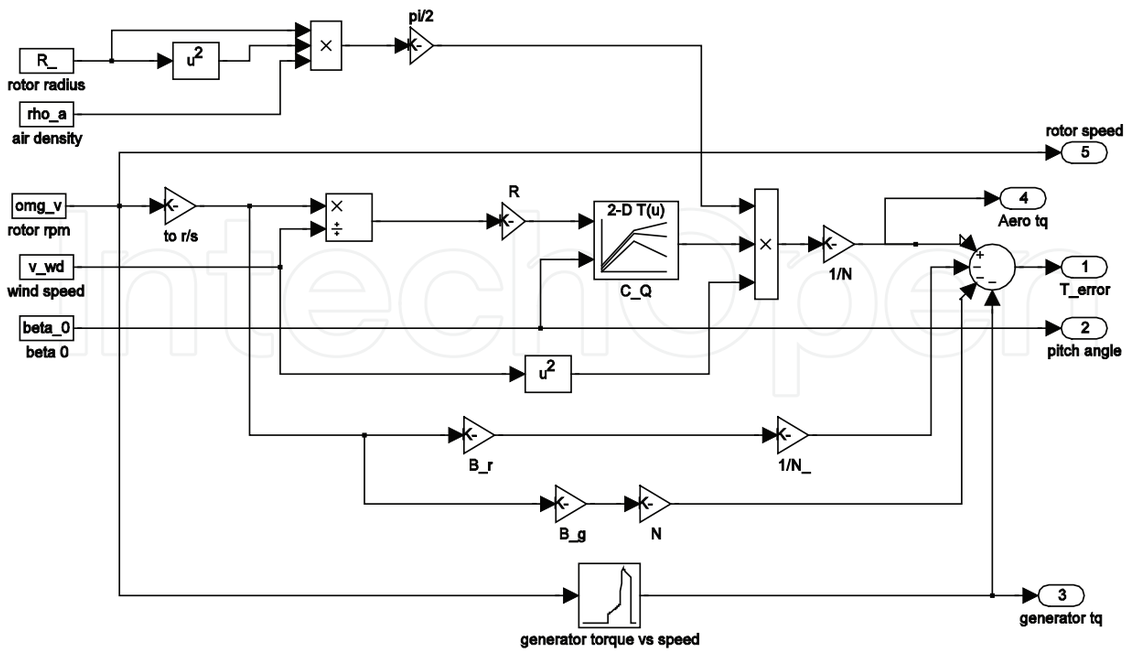

Fig. 12. Simulink model of Eq. (15) in the below rated wind speed region

data for C_Q and T_g. A numerical method using an optimization algorithm can be applied to solve this problem. Fig. 12 shows a Matlab/Simulink© model of Eq. (15). The #4 output ('Aero tq') in this figure corresponds to the first term of Eq. (15). The other blocks below this represent the remaining terms of Eq. (15). Therefore, the #1 output ('T_error') is the total sum of terms in left side of Eq. (15). An optimization algorithm which minimizes the magnitude of 'T_error' can be applied to find an appropriate rotor speed ('omg_v' in Fig. 12) for a fixed wind speed ('v_wd') and a fixed pitch angle ('beta_0'). By iterating the above procedure for wind speeds in the whole below rated region, an appropriate rotor speed schedule similar to Fig. 13 can be sought out. Exactly the same algorithm as the above is applied to find a pitch angle variation in the above rated wind speed region, where the rotor speed is fixed at rated speed. Fig. 13 shows full sets of three variables, (Ω_r, v, β), which are obtained using the above algorithms. The trajectory in this figure defines the steady state operating point for each wind speed from the cut-in to the cut-out wind speed envelope.

Fig. 14 provides some additional insights on the steady state operations of Fig. 13. Note how the power coefficient, C_P, varies with changes in wind speed, pitch angle, and rotor speed. A torque schedule similar to the one shown as a thick solid line in Fig. 10 is applied in this analysis. As the wind speed increases from zero to $v_{D'}$ in Fig. 10, the wind turbine starts to rotate and then reaches and stays for a while at the max-C_P operational state. Because of the torque schedule of Fig. 10, the magnitude of Cp decreases in a transition region from the max-C_P value and goes toward zero in the above rated wind speed region, being inversely proportional to the third power of wind speed as explained in Section 2.2. Note also how C_P varies with the pitch angle. In this figure, try to identify the matching rotor speeds, Ω_{min}, Ω_1, Ω_2, and Ω_{rated}, of Fig. 10. The final plot of Fig. 14 shows the variation of tip speed ratio, λ, as a function of wind speed.

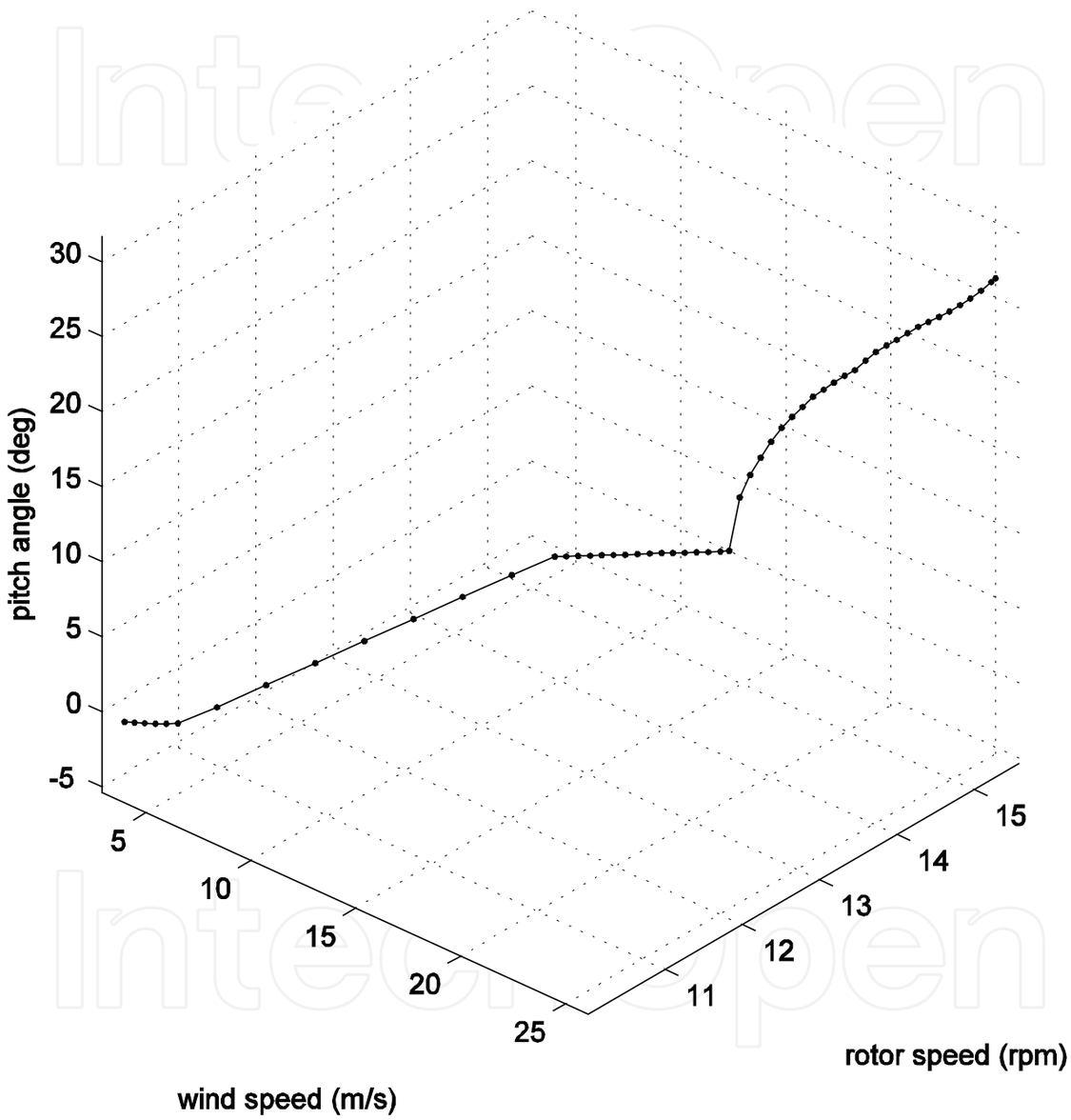

Fig. 13. Locus of operating point variation with wind speed

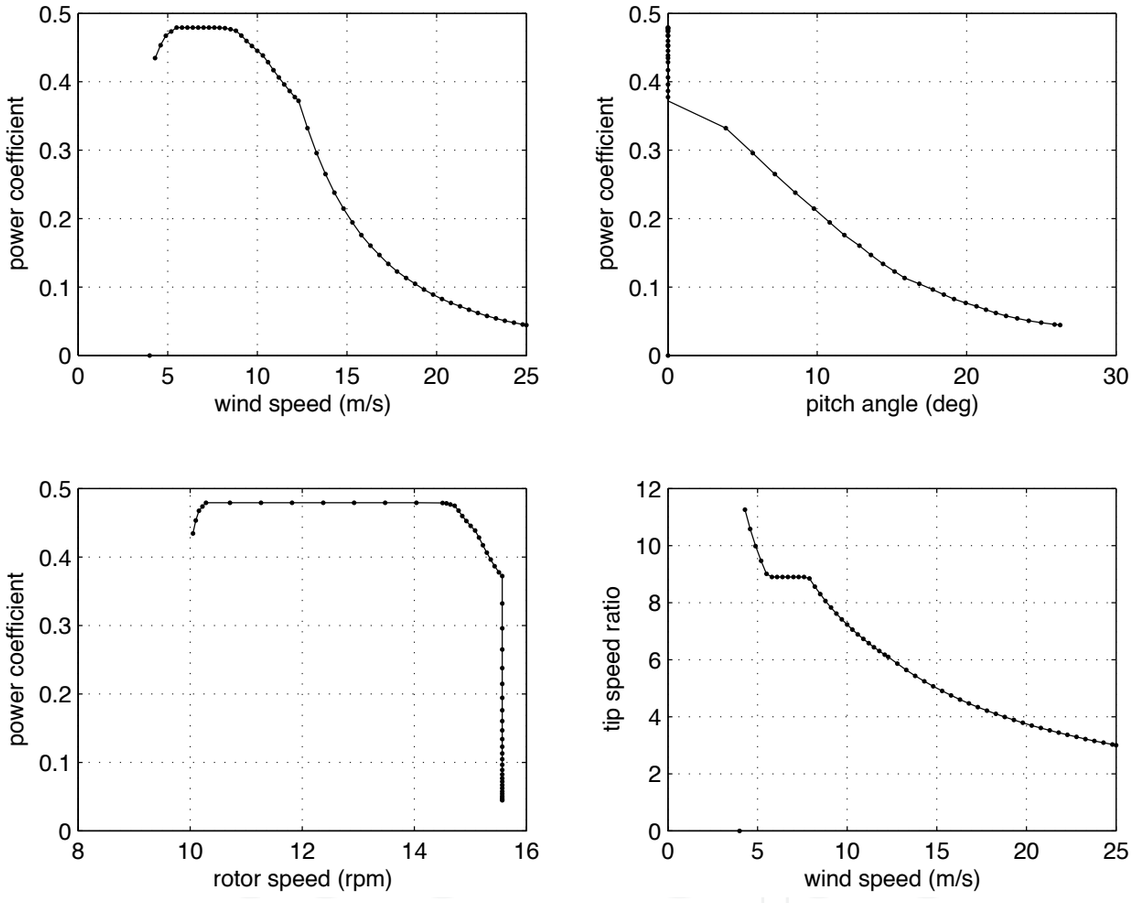

Fig. 14. Variation of C_P and λ with changes in wind speed, pitch angle, and rotor speed

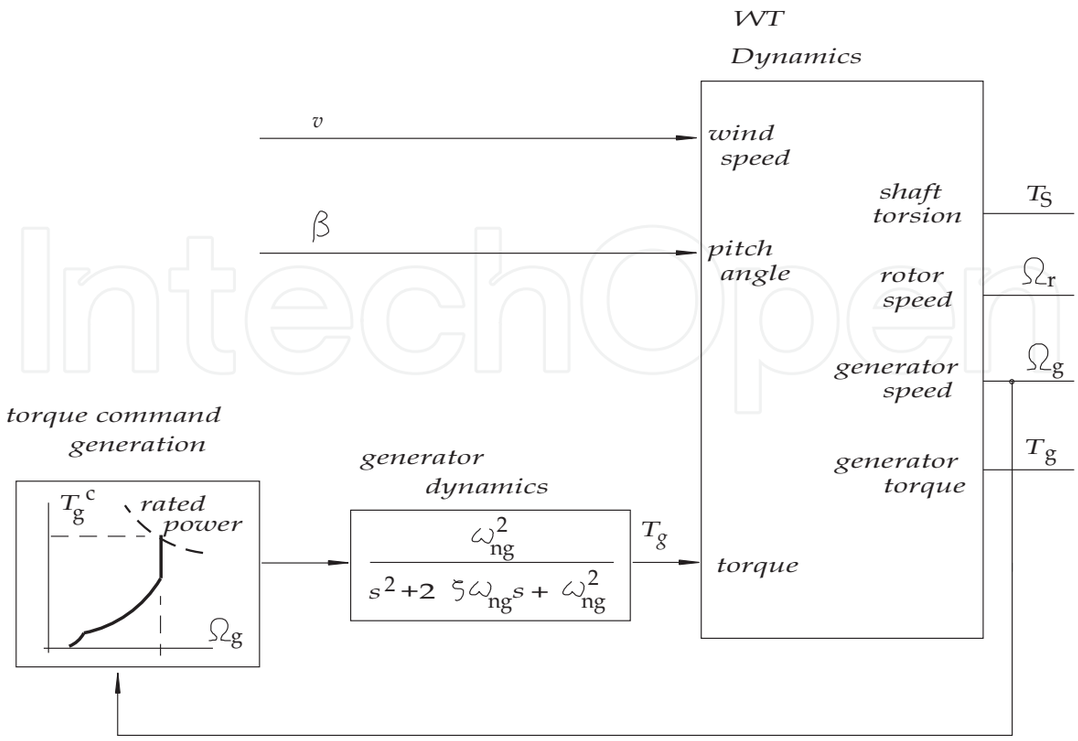

Fig. 15. Schematic open pitch loop structure of wind turbine

3.4 Dynamic characteristic change with varying wind speed

A wind turbine should be maintained to operate on a locus of Fig. 13 for varying winds if it produces electric power as specified in the power curve. Then, would the dynamic characteristics of the wind turbine be the same for all operational points of this locus? If different, by how much would they differ? It is important to understand these characteristics well for a successful pitch control system design, which will be covered in the next section. Fig. 15 shows a schematic open pitch loop structure. Generator torque control is implemented by high speed switching power electronics. Therefore, it has much faster dynamics than a pitch control loop. In Fig. 15, the generator torque control system is modeled as a second order system of Eq. (9) and controlled as specified with the torque-rotor speed schedule table. The 'WT Dynamics' block of Fig. 15 can be represented with the drive train model of Eq. (12), which is easily programmed with Matlab/Simulink©. A linearized model for each operating point, (Ω_{ro}, v_o, β_o), on the locus of Fig. 13 can be found as follows:

$$\begin{aligned} \dot{\mathbf{x}} &= A\mathbf{x} + B\mathbf{u} \\ \mathbf{y} &= C\mathbf{x} + D\mathbf{u} \end{aligned} \tag{16}$$

where $\mathbf{x} = \left[x_1 \;\; x_2 \;\; x_3 \;\; x_4 \;\; x_5 \;\; x_6\right]^T = \left[\delta\Theta_g \;\; \delta\Theta_r \;\; \delta\Omega_r \;\; \delta\Omega_g \;\; \delta T_g \;\; \delta(dT_g/dt)\right]^T$

$\mathbf{u} = \left[u_1 \;\; u_2\right]^T = \left[\delta v \;\; \delta\beta\right]^T$

$\mathbf{y} = \left[y_1 \;\; y_2 \;\; y_3 \;\; y_4\right]^T = \left[\delta T \;\; \delta\Omega_r \;\; \delta\Omega_g \;\; \delta T_g\right]^T$.

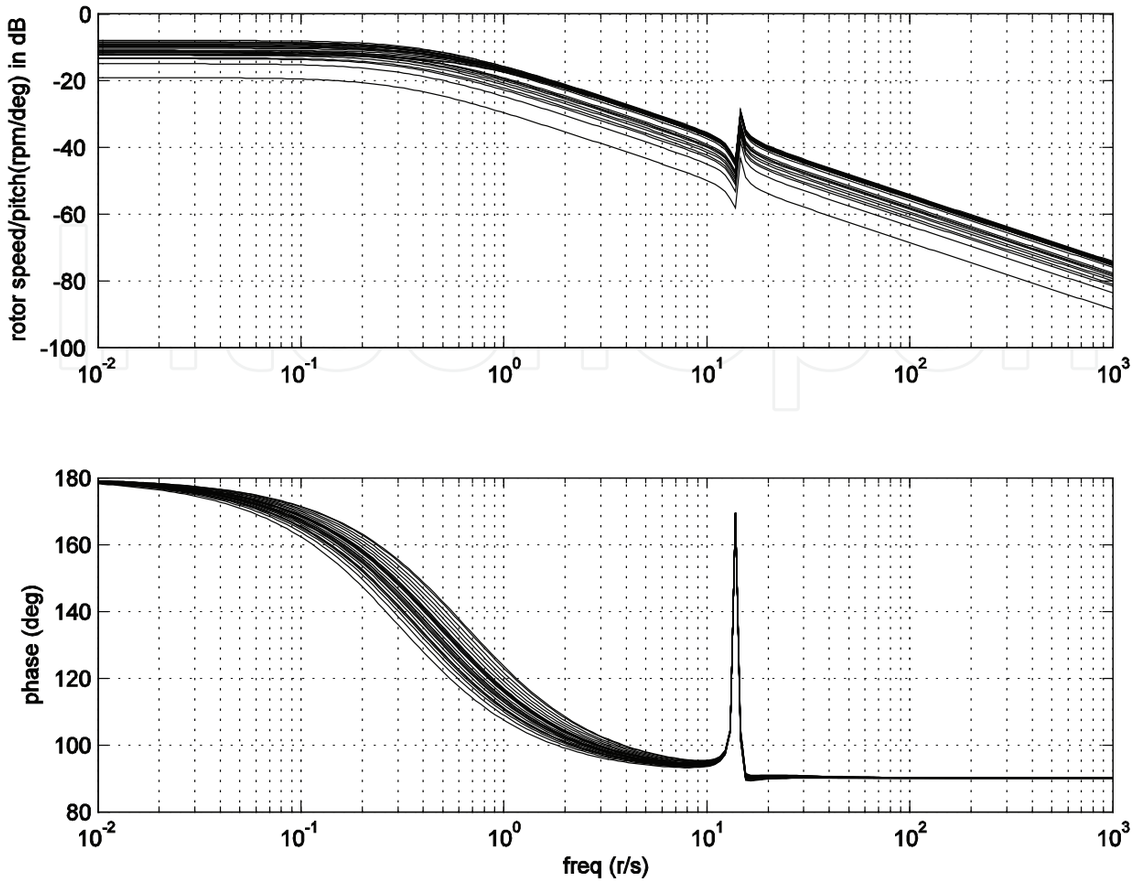

Fig. 16. Frequency response of $G_{22}(s)=\delta\Omega_r(s)/\delta\beta(s)$ for operating points in the above rated wind speed region

Θ_g and Θ_r in the above equation are the rotational displacement of the generator and rotor. Note that the linear model of Eq. (16) is meaningful only in the vicinity of (Ω_{ro}, v_o, β_o).

A transfer function of rotor speed for the pitch angle input, $G_{22}(s)=\delta\Omega_r(s)/\delta\beta(s)$ can be obtained from the linear model of Eq. (16). This transfer function is important in the pitch controller design. A sample of frequency response of this transfer function for a multi-MW wind turbine is shown in Fig. 16. Frequency responses only for the above rated wind speed region are displayed, because a pitch control is active only in this region. Overall, it behaves like a first order system but has some variations in DC gain and low frequency pole location with different operating conditions. The difference of DC gain for each operating point comes from the pitch effectiveness variation with wind speed. As already shown in Fig. 11, the pitch effectiveness, k_β (the plot with '◊' in Fig. 11), becomes larger with an increase of wind speed. Therefore, the frequency responses having larger DC gain in Fig. 16 correspond to those at high wind speed operating points. The peaks at around 16 r/s represent the torsional vibration mode of the drive train. As mentioned in the above, the dynamics of a wind turbine is similar to a first order dynamic system. Because of the huge moment of inertia of three blades for a multi-MW machine, it usually takes more than several seconds to reach steady state operation for abrupt changes in wind speed or pitch angle. Fig. 17 shows changes in dominant pole (i.e. pole of the first order system) locations with different

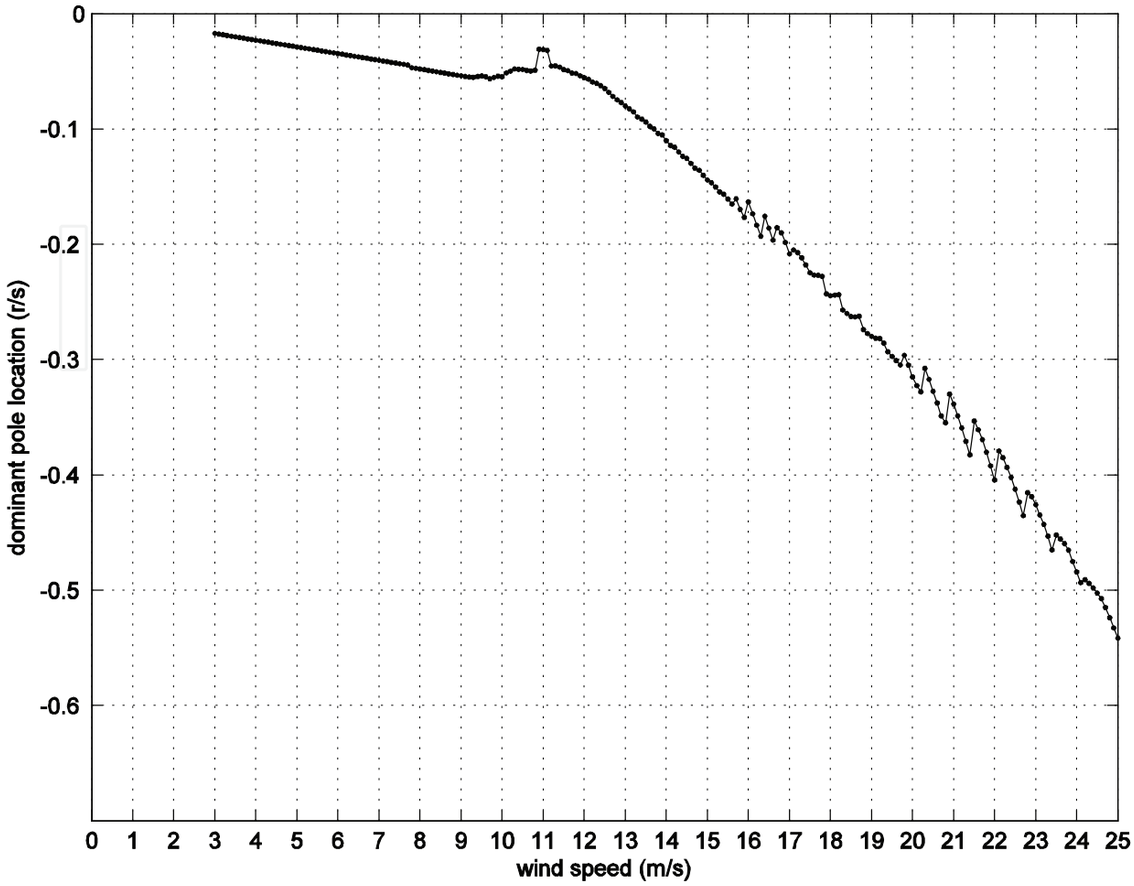

Fig. 17. Variation of dominant pole locations with wind speed for a multi-MW wind turbine

operating conditions. A wind turbine having the operating locus of Fig. 13 has stable but very slow dynamics, especially in the low wind speed region. In designing a pitch controller at around the rated wind speed region, the characteristics of slow dynamics and low DC gain should be considered.

4. Control system design

4.1 Control system design requirements

A control law structure for power curve tracking is introduced in Fig. 7. It consists of two feedback loops. One is the generator torque control loop, which is covered in Section 3, and the other is the pitch control loop. As mentioned earlier, depending on wind speed, there are two control regimes. In the below rated wind speed region, the pitch angle is fixed at β_0 and the generator torque is controlled to maintain max-Cp operation in the face of turbulence. But in the above rated region pitch control is active to regulate the rotational speed of the rotor to the rated rpm while maintaining generator torque at the rated value. Therefore, the electric power of a wind turbine is regulated as rated in this region. The design of the pitch control loop of Fig. 7 is a matter of selecting suitable PI gains to make the control system satisfy some design criteria. How to set the pitch control system bandwidth is one of the design criteria.

The bandwidth of a wind turbine control system should be fast enough to extract the wind power in a turbulent wind spectrum. Assuming that Eq. (4) in Section 2.1 can be approximated as

$$\Phi_{vv}(\omega)=\frac{4\sigma_u^2 L_u/\overline{v}}{\left(1+70.8\left(\omega L_u/(2\pi\overline{v})\right)^2\right)^{5/6}}\simeq\frac{4\sigma_u^2 L_u/\overline{v}}{1+70.8\left(\omega L_u/(2\pi\overline{v})\right)^2}, \tag{17}$$

a turbulent wind could be modelled using a first order Markov process (Gelb, 1974). The power spectral density of the output signal of the first order Markov process, $y(t)$, for the input, $x(t)$, i.e. white noise, is given as

$$\Phi_{yy}(\omega)=\left|G(j\omega)\right|^2\Phi_{xx}(\omega)=\frac{k^2}{\omega^2+\beta_1^2}=\frac{(k/\beta_1)^2}{1+(\omega/\beta_1)^2} \tag{18}$$

where $G(s)= k/(s+\beta_1)$ is a first order low pass filter system. Comparing Eq. (18) with Eq. (17), one can notice that a turbulent wind can be generated by filtering a white noise with a first order low pass filter which has a cut-off frequency of

$$\beta_1=\frac{2\pi\overline{v}}{\sqrt{70.8}L_u}. \tag{19}$$

Therefore, a design criterion for the bandwidth of a wind turbine system is that it should be larger than β_1, which has values in the range of 0.0196 ~ 0.148 r/s, depending on the type of terrain (see Table 1, Eq. (3), and Eq. (4): 0.148 r/s for a mean wind speed of 25 m/s in a flat desert or rough sea). However, the pitch control loop bandwidth cannot be set too high because of non-minimum phase (NMP) zero dynamics of the wind turbine. Fig. 18 shows the frequency response of the rotor rpm for the pitch demand. This plot is obtained from a linearized aeroelastic model of a multi-MW wind turbine at a wind speed of 13 m/s. An abrupt phase change of 360 degrees at around 2 r/s implies the existence of NMP zero dynamics of

$$\frac{s^2-2\zeta\omega_z s+\omega_z^2}{s^2+2\zeta\omega_z s+\omega_z^2} \tag{20}$$

in the transfer function of $G_{22}(s)=\delta\Omega_r(s)/\delta\beta(s)$. This NMP zero dynamics is related with the first mode of tower fore-aft motion (Dominguez & Leithead, 2006). This is a common characteristic of most multi-MW wind turbines. It is well known that a NMP zero near to the origin in the s-plane sets a limit for the crossover frequency (~bandwidth) of the loop gain transfer function. Therefore, the frequency of the NMP zero coming from the tower fore-aft motion determines an upper bound of the pitch control loop bandwidth.

4.2 Pitch controller design and gain scheduling

There are two design parameters, i.e. k_p and k_I/k_p, for the pitch control system structure of Fig. 7. As discussed in the former section, these parameters are to be selected such as to meet the crossover frequency requirement. The loop gain transfer function from the point ① to the point ② in Fig. 7 is the most important in the pitch controller design and has the following form:

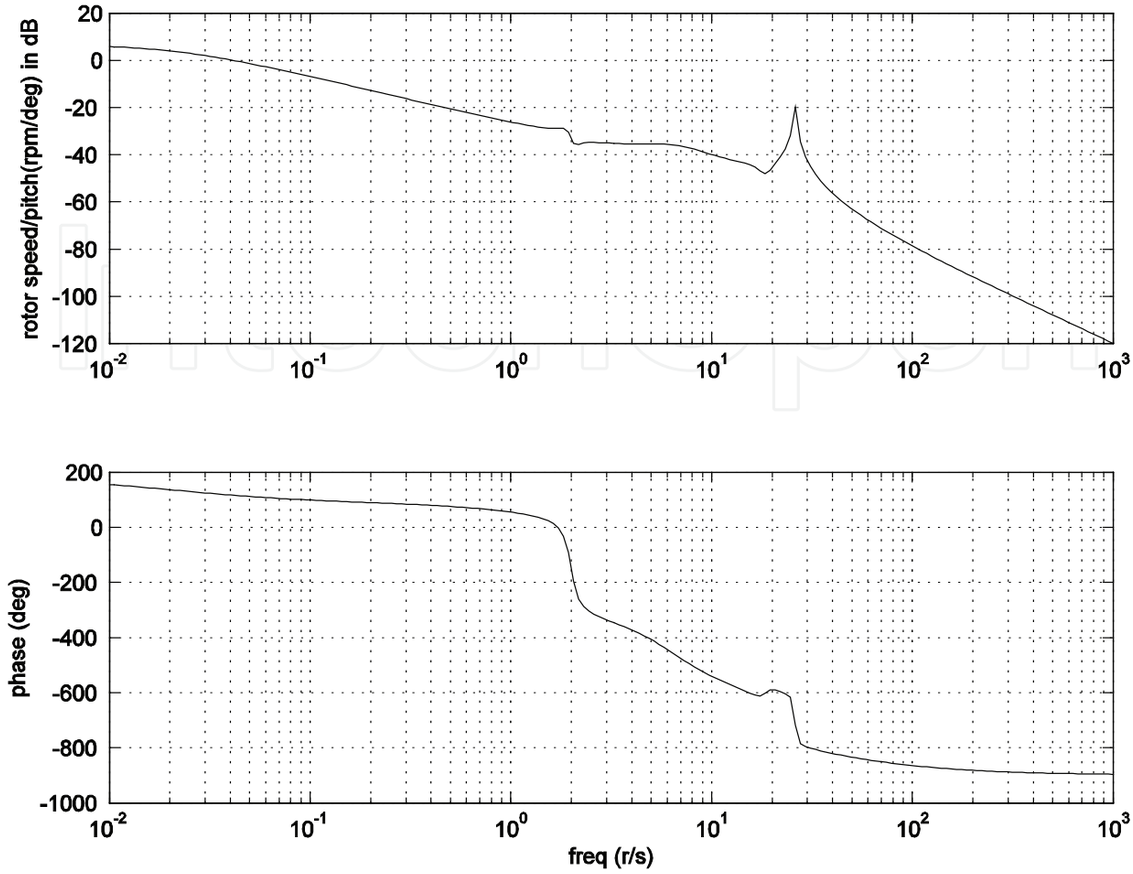

Fig. 18. Frequency response of rotor speed for the pitch demand ($G_{22}(s)=\delta\Omega_r(s)/\delta\beta(s)$) from an aeroelastic model of a multi-MW wind turbine at 13 m/s

$$L(s) = G_{22}(s)\left(\frac{1}{1+\tau_p s}\right)\left(k_P + \frac{k_I}{s}\right) = G_{22}(s)\left(\frac{1}{1+\tau_p s}\right)\left(\frac{k_p(s+k_I/k_p)}{s}\right). \quad (21)$$

Fig. 19 shows the frequency response of the pitch loop gain transfer function at a wind speed of 22.8 m/s for a multi-MW wind turbine, which is obtained using the linearized drive train model of Eq. (12). A crossover frequency of 1 r/s and phase margin of 90° are achieved for the selection of k_p=-5.844 *(deg/rpm)* and k_I/k_p=0.55 *(1/s)*. Increasing (decreasing) the magnitude of the proportional gain, k_p, from 5.844 results in a higher (lower) crossover frequency than 1 r/s. Then, how does the parameter, k_I/k_p affect the pitch loop design? As explained in Section 3.4 (see Fig. 16), the dynamics of $G_{22}(s)=\delta\Omega_r(s)/\delta\beta(s)$ can be approximated as a first order transfer function, the pole of which varies with the wind speed as shown in Fig. 17 for a multi-MW machine. By referring to Fig. 20, which is a root-locus plot for the pitch control loop, the question of how to set the parameter k_I/k_p is answered. Depending on the selection of k_I/k_p, the shape of the root-locus differs greatly. If this parameter is chosen to be smaller than the magnitude of the open loop pole in Fig. 17 for the design wind speed, it would be difficult to achieve the requirement on the crossover frequency of 1 r/s, even when applying very high proportional gain.

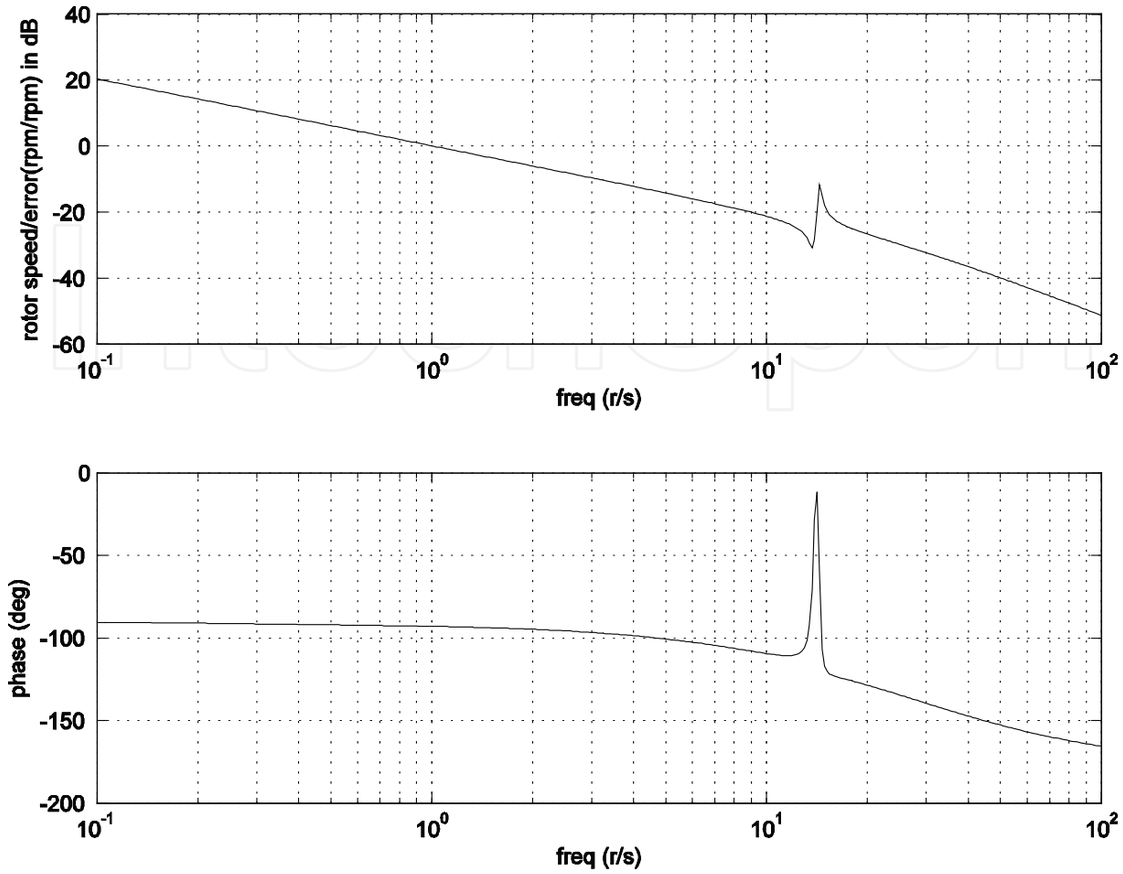

Fig. 19. Frequency response of pitch loop gain transfer function at 22.8 m/s

Successful completion of a pitch loop design for a certain design point (for example, 22.8 m/s in the above) does not guarantee the same level of design for any other design point, because the pitch effectiveness, k_β, varies with the wind speed (see the plot with '◊' in Fig. 11). As shown in this figure, the pitch effectiveness in the rated wind speed region is the lowest, which matches the frequency response of $G_{22}(s)=\delta\Omega_r(s)/\delta\beta(s)$ having the lowest DC gain in Fig. 16. If the same pitch controller gains as those for 22.8 m/s are used in the rated wind speed region, the crossover frequency of the pitch loop would be so low that there might be a large excursion of rotor speed from rated. A gain scheduling technique can be applied to compensate the DC gain variation with the wind speed. The PI controller in Eq. (21) multiplied by a scheduled gain, $k_G(\beta)$, is given as

$$k(s)=\frac{\beta^C(s)}{E(s)}=k_G(\beta)\left(k_P+\frac{k_I}{s}\right)=k_G(\beta)\cdot\frac{k_p(s+k_I/k_p)}{s}. \tag{22}$$

It is common to schedule the gain, k_G, as a function of pitch angle, β as in Eq. (22), because the wind speed is not only difficult to estimate but also too high frequency for a gain scheduling operation. A sample of scheduled gain, $k_G(\beta)$, for a multi-MW wind turbine is shown in Fig. 21. These gains are determined from the plot of the pitch effectiveness, k_β, with the pitch angle, which is similar to the plot with '◊' in Fig. 11. However, too much

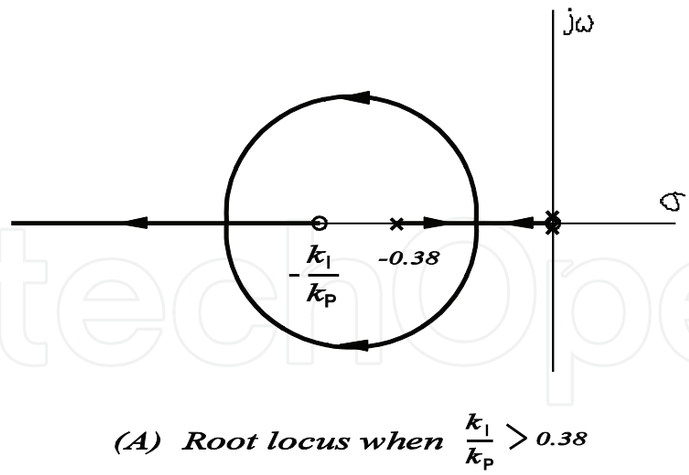

(A) Root locus when $\frac{k_I}{k_P} > 0.38$

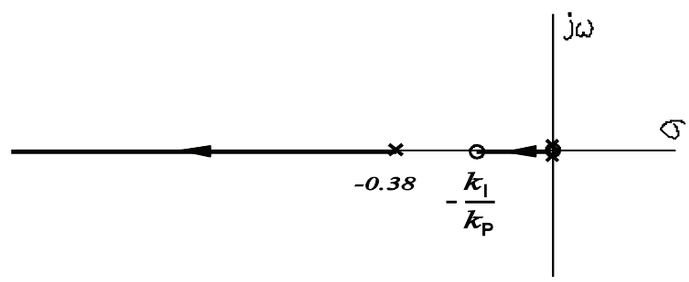

(B) Root locus when $\frac{k_I}{k_P} < 0.38$

Fig. 20. Change of root locus of the pitch control loop depending on k_I/k_p selection

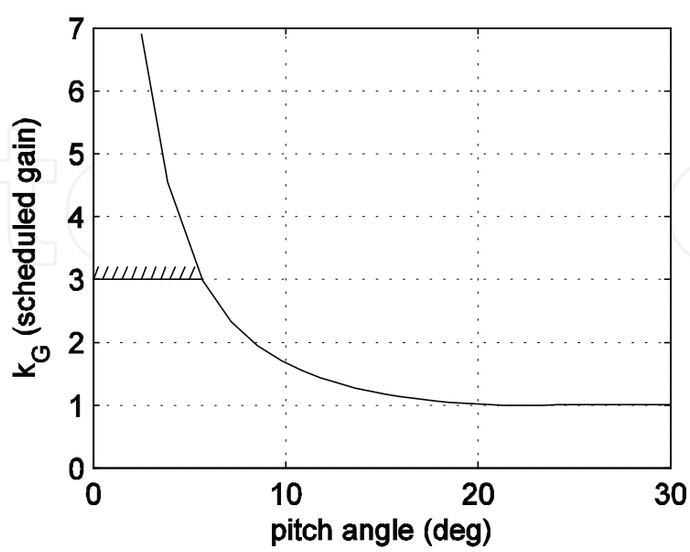

Fig. 21. Gain scheduling as a function of pitch angle

scheduled gain in the rated wind speed region might result in large mechanical loads on the blades and tower. Therefore, it would be reasonable to limit the scheduled gain to a certain value as depicted in Fig. 21. The appropriate limit should be determined through a full nonlinear simulation covering aeroelastic behaviour of structural loads.

As pointed out in Section 2.2 (see Fig. 8), the pitch actuator has saturation in speed and displacement. If integral control is used with the actuator having travel limits, a well-known integrator windup problem arises. This might cause too large an excursion in rotor rpm from the rated value or might make the pitch system unstable. By preventing integral action when the pitch is at the limit, which is called integrator anti-windup, this problem can be solved. Discrete implementation of an anti-windup PI controller is shown in Fig. 22, where the approximation of integral action is made by the following relations. For the sampling interval T, the output of the PI controller of Eq. (22) at the k-th sampling time, $\beta^C(kT)$, is given by

$$\beta^C(kT) = k_G(\beta)\left(k_P e(kT) + k_I \int_0^{kT} e(\tau)d\tau\right). \tag{23}$$

The output of the PI controller at $t=(k-1)T$, $\beta^C((k-1)T)$, can be obtained in a similar way. Then, the following relation holds:

$$\Delta\beta_k^C = \beta^C(kT) - \beta^C((k-1)T) \simeq k_G(\beta)\left\{k_P\{e(kT) - e((k-1)T)\} + k_I T\frac{e(kT) + e((k-1)T)}{2}\right\}. \tag{24}$$

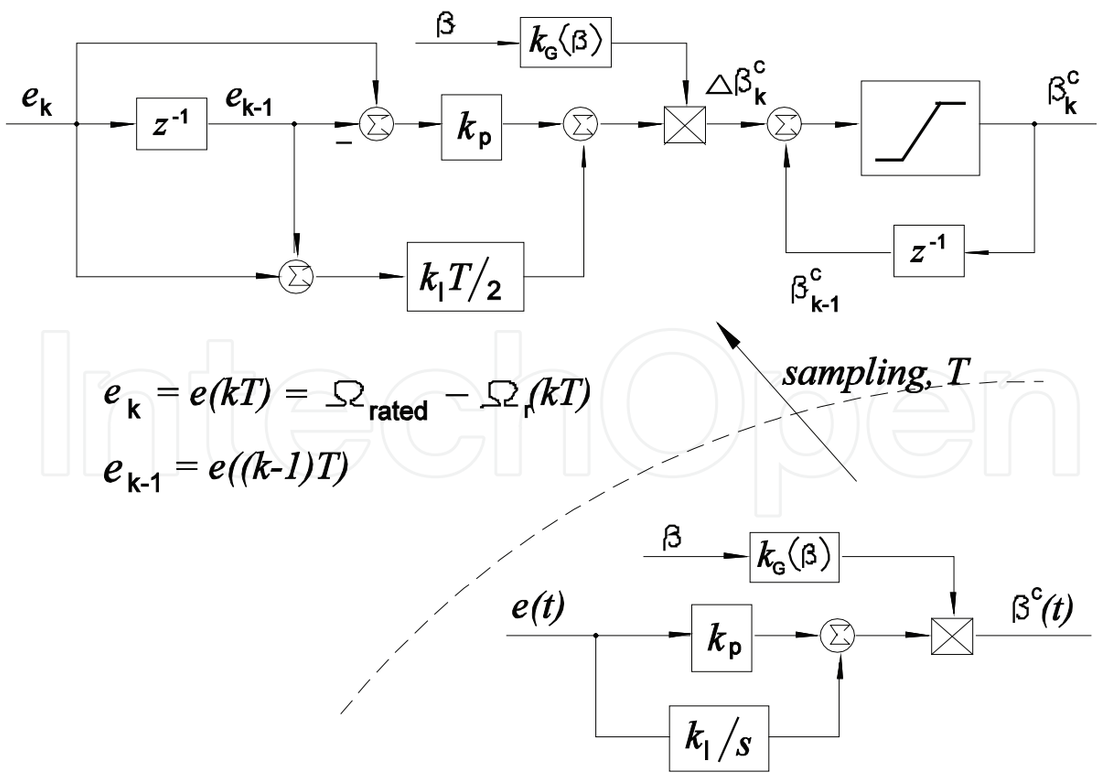

Fig. 22. Discrete PI controller with the integrator anti-windup

Fig. 22 is just a graphical representation of Eq. (24) with the integral anti-windup function, which is implemented with a limiter.

This section concludes by introducing simulation results which were obtained by applying the above pitch control system for a mean wind speed of 15 m/s with a turbulence intensity of 17.5 %. These are shown in Fig. 23 and Fig. 24 and were obtained using GH Bladed© (Bossanyi, 2009) for a 2 MW wind turbine. A generator torque schedule similar to A-B-C-D-E-F of Fig. 10 is applied in both simulations. A gain scheduling technique is applied, in which the maximum gain is limited to 7. Too much gain scheduling in the rated wind speed (small pitch) region might result in large fluctuations in rotor speed and an increase in mechanical loads on the wind turbine structure. The results in Fig. 23 are for a pitch loop design of 0.8 r/s crossover frequency, while those in Fig. 24 are for 1.7 r/s. The first window in these figures represents the wind speed in m/s and the second shows the rotor speed in rpm. After these, the pitch angle (deg), generator torque (kNm), and output power (kW) are shown. The final 4 windows in these figures show the structural response of the blade and tower. The first two plots show the bending moments (MNm) at the root of the #1 blade in the in-plane and out-of-plane direction (see Section 4.4 for the definition of these directions). The next two plots show the root bending moments (MNm) of the tower in the side-side and fore-aft direction. As the pitch loop bandwidth (~crossover frequency) is designed to be higher, the rotor speed fluctuations over the rated rpm become much smaller (compare the second plots of Fig. 23 and Fig. 24). This is the anticipated consequence because the high bandwidth pitch control system tries to manage the rpm errors tightly compared to the low bandwidth system. Noting the relationship (power)=(generator torque)x(rotor speed), compare also the responses of output power in the fifth plot of the figure. While the difference of performance response such as rotor speed or power is very comparable in Fig. 23 and Fig. 24, it is difficult to differentiate between the structural response such as blade or tower bending moment in these figures. The damage equivalent loads (DEL), M_{eq}, can be a quantitative measure which shows differences between the two mechanical load responses and is given by

$$M_{eq} = \left(\frac{\sum_k (M_k)^m n_k}{n_{tot}} \right)^{1/m} \tag{25}$$

where n_k is the number of cycles in mechanical load range M_k and n_{tot} is the total number of cycles in a mechanical load signal. m in this equation is the material specific number, for example m=3.5 for a steel tower structure and m=10 for a fiber glass blade (Bossanyi, 2008). The larger the DEL value, the more prone to end up in fatigue failure. The statistical data of performance response and DEL data of structural load response for the two cases of different crossover frequencies are summarized in Table 3. A remarkable performance improvement is expected for the pitch control system design with the 1.7 r/s crossover frequency compared to the system with the frequency of 0.8 r/s. As the rotor fluctuates more around the rated rpm, the DEL of the blade bending moment in the out-of-plane direction and the tower root bending moment in the fore-aft direction becomes larger. However, the effects of these on the in-plane blade loads and the side-side tower loads seem to be minor.

4.3 Wind speed estimation and feedforward pitch control

The dynamic response of a multi-MW wind turbine to the wind is slow. Assuming that the crossover frequency of a pitch control loop is around 1 r/s, it would take more than 2

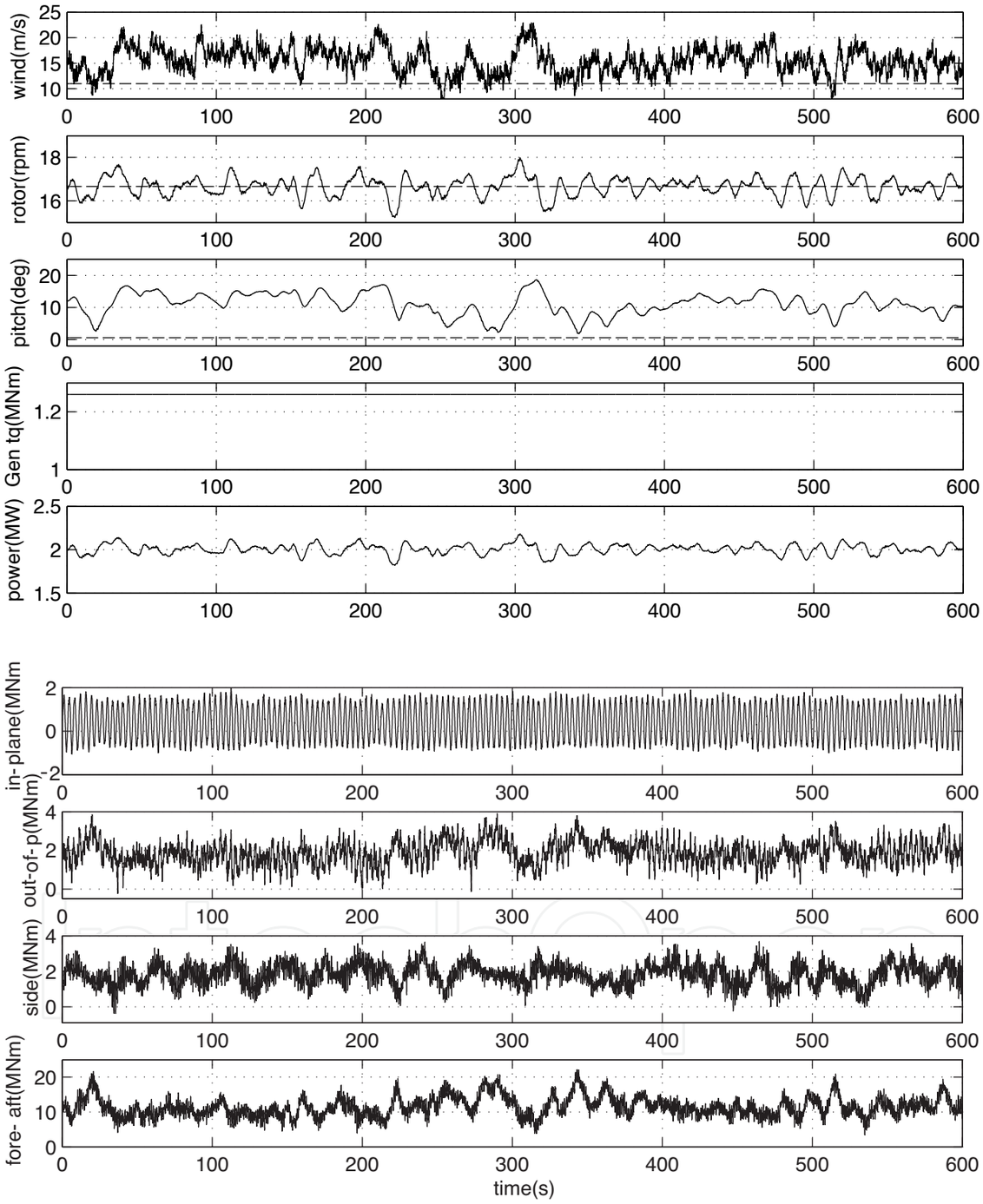

Fig. 23. Performance and structural response in time domain for a turbulent wind when the crossover frequency of the pitch loop is 0.8 r/s

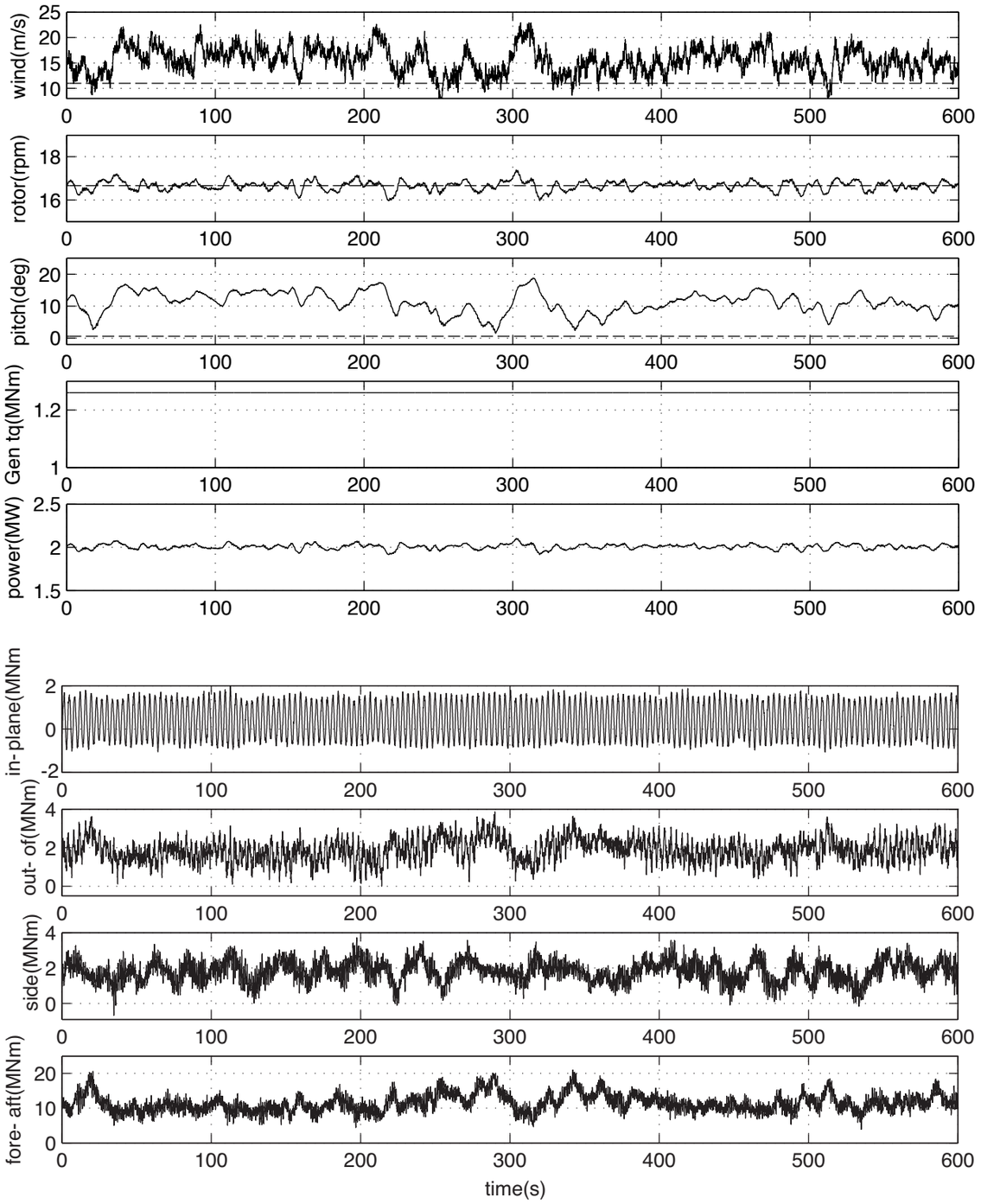

Fig. 24. Performance and structural response in time domain for a turbulent wind when the crossover frequency of the pitch loop is 1.7 r/s

seconds to reach a steady state for a step change in wind speed. A pitch control system will respond in the right way only after some error in rotor speed for the change of wind speed is developed. If the pitch actuation system is commanded with the wind speed information instead of the rotor speed error, then the fluctuation of rotor speed can be decreased by anticipating pitch action.

Feedforward pitch control using wind speed estimation improves the performance of power output regulation for turbulent wind operation. Fig. 25 shows a schematic structure of a feedforward pitch control. It consists of an aerodynamic torque estimator, a 3-dimensional look-up table which outputs the estimated wind speed, and two feedforward gains. The aerodynamic torque of Eq. (11), which is rewritten as Eq. (26), is the basic relation for the wind speed estimation:

$$T_a = \frac{1}{2}\rho\pi R^3 \frac{C_P(\lambda,\beta)}{\lambda} v^2 = \frac{1}{2}\rho\pi R^3 C_Q(\lambda,\beta) v^2 \,. \tag{26}$$

The above equation has 4 variables, namely the aerodynamic torque T_a, rotor speed Ω_r (see Eq. (8)), pitch angle β, and wind speed v. Among these variables, the rotor speed and pitch angle are measurable. Therefore, if estimation of the aerodynamic torque is possible, then the wind speed can be pre-calculated and presented as a 3-dimensional look-up table as depicted in Fig. 25. In high wind speed ranges up to cut-out, the relationship between the

Crossover Frequency, w_c (r/s)	Performance data				Structural loads data (DEL)			
	Rotor (rpm)		Power (kW)		Blade (MNm)		Tower (MNm)	
	mean	std.	mean	std.	in-plane	out-of-plane	side-side	fore-aft
w_c = 0.8 (A)	16.657	0.441	2007.8	58.17	2.119	2.334	1.457	5.582
w_c = 1.7 (B)	16.659	0.215	2008.1	28.32	2.124	2.203	1.452	5.276
(B-A)/A(%)	0.01	-51.3	0.01	-51.3	0.24	-5.56	-0.34	-5.48

Table 3. Comparison of performance and structural response data for different crossover frequencies

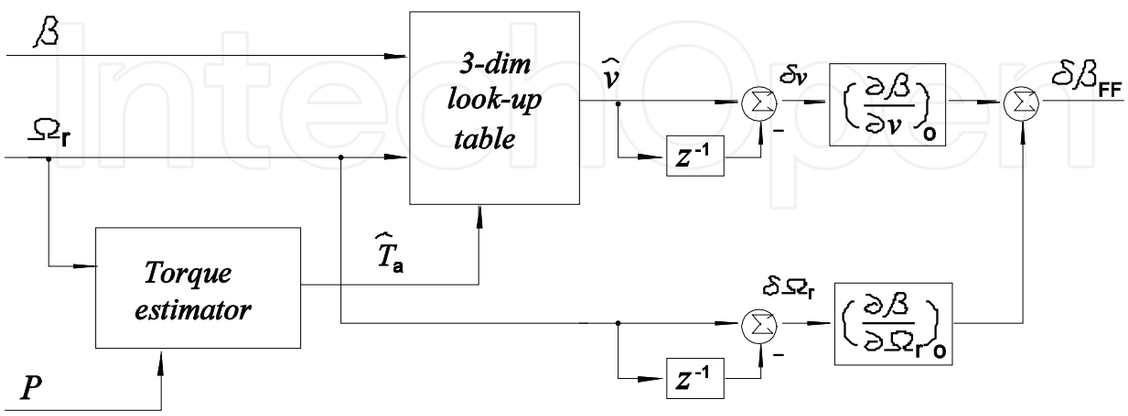

Fig. 25. Schematic diagram of the feedforward pitch control

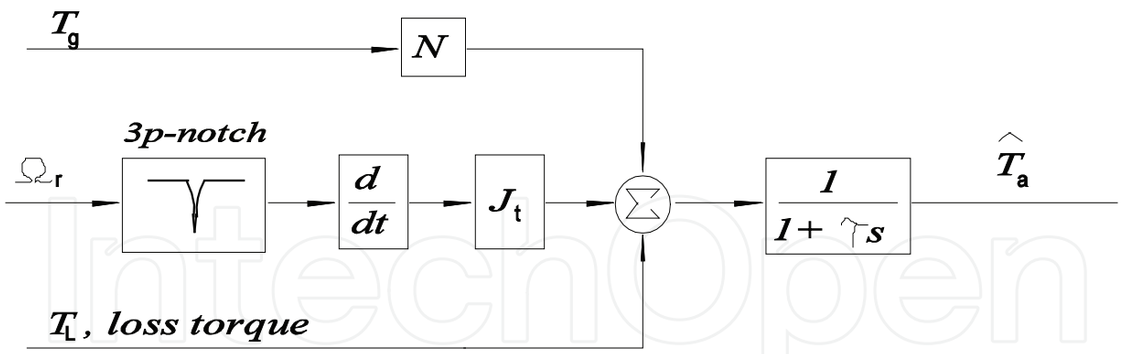

Fig. 26. Aerodynamic torque estimator based on a simple drive train model

aerodynamic torque and the wind speed in Eq. (26) is one-to-one where the wind turbine is operating at a large pitch angle. However, this relation is broken on operating near to the rated wind speed region where the pitch is small, because of the concaveness of $C_Q(\lambda,\beta)$ in Eq. (26). In this region, there could be two solutions for the wind speed for a certain aerodynamic torque. In this case, the smaller wind speed, which is near to the rated wind speed, is the normal solution, while the larger one corresponds to the wind speed at stall condition.

There are several ways of estimating the aerodynamic torque. The simplest one uses the drive train model of Eq. (12). The two equations in Eq. (12) are combined to give

$$J_t \frac{d\Omega_r}{dt} = T_a - NT_g - T_L \tag{27}$$

where $J_t = J_r + N^2 J_g$ and T_L is a mechanical loss torque. All the viscous frictional terms in Eq. (12), such as $B_r\Omega_r$ are combined in the mechanical loss. A schematic of a torque estimator using this equation is shown in Fig. 26. A low pass filter is used to suppress the high frequency noise generated from the differentiation of measured rotor speed. Filtering out the 3p (1p=rotational frequency) or drive train resonant frequency component in the rotor speed signal might be necessary (van der Hooft & van Engelen, 2003). The use of a dynamic estimator such as a Kalman filter is another option. Augmenting the unknown input, T_a, in the state vector, Eq. (27) becomes

$$\begin{aligned} \dot{x} &= \begin{Bmatrix} \dot{\Omega}_r \\ \dot{T}_a \end{Bmatrix} = \begin{bmatrix} 0 & 1/J_t \\ 0 & 0 \end{bmatrix} \begin{Bmatrix} \Omega_r \\ T_a \end{Bmatrix} + \begin{pmatrix} -N/J_t \\ 0 \end{pmatrix} T_g + \begin{pmatrix} -1/J_t \\ 0 \end{pmatrix} T_L + \begin{pmatrix} -N/J_t \\ 1 \end{pmatrix} w_g \\ y &= \begin{bmatrix} 1 & 0 \end{bmatrix} \begin{Bmatrix} \Omega_r \\ T_a \end{Bmatrix} + v \end{aligned} \tag{28}$$

where w_g and v are input process and sensor noise. The state estimator can be designed by combining Eq. (28) with a measurement update term:

$$\dot{\hat{x}} = \begin{Bmatrix} \dot{\hat{\Omega}}_r \\ \dot{\hat{T}}_a \end{Bmatrix} = \begin{bmatrix} 0 & 1/J_t \\ 0 & 0 \end{bmatrix} \begin{Bmatrix} \hat{\Omega}_r \\ \hat{T}_a \end{Bmatrix} + \begin{pmatrix} -N/J_t \\ 0 \end{pmatrix} T_g + \begin{pmatrix} -1/J_t \\ 0 \end{pmatrix} T_L + L\left(\Omega_r - \hat{\Omega}_r\right) \tag{29}$$

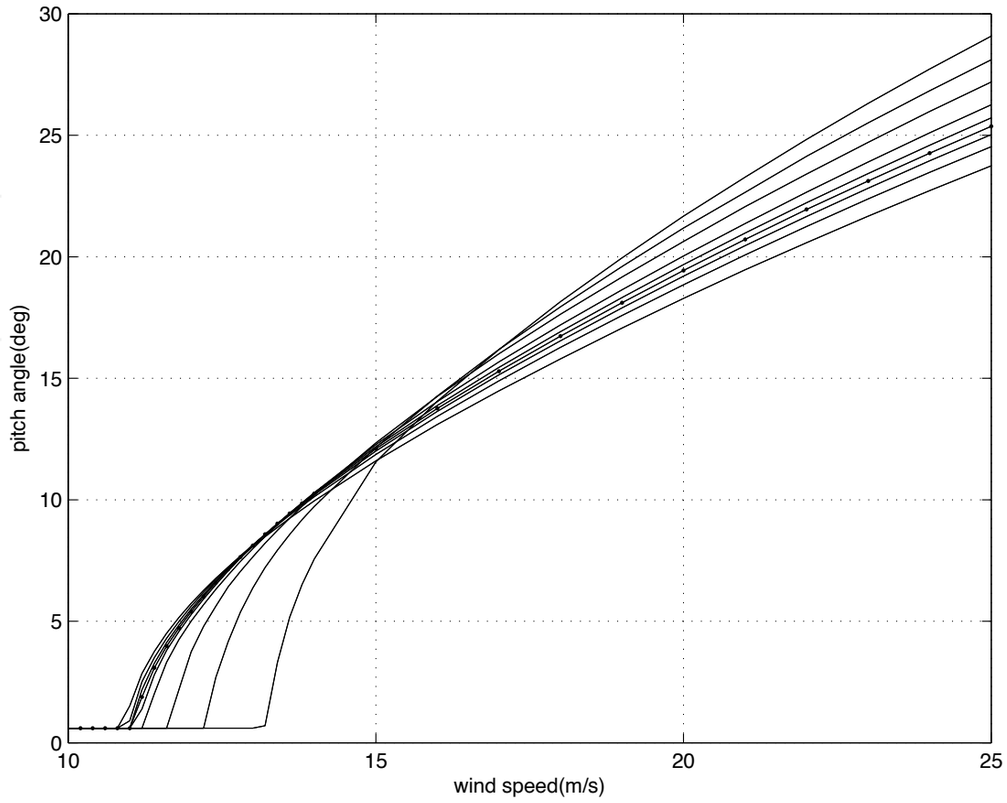

Fig. 27. Family of a set of parameters, (Ω_{ro}, v_o, β_o), which produce the rated power

where the variables with hat are estimated and L is the estimator gain. The estimated torque and two other measurable variables, i.e. rotor speed and pitch angle, are input to a 3-dimensional look-up table, and then the pre-calculated wind speed can be obtained. Note that the estimated wind speed from the 3-dimensional table is not real. It is so called effective wind speed, which is the spatial average of the wind field over the rotor plane with the wind stream being unaffected by the wind turbine (Ostergaard et al., 2007).

The purpose of feedforward pitch control is to minimize rotor speed fluctuation so that good quality of power regulation is achieved. The wind turbine would generate the rated power P_{rated}, for a set of parameters, (Ω_{ro}, v_o, β_o), which can be sought by solving the equation:

$$P = \frac{1}{2}\pi R^2 C_P(\lambda, \beta) v^3 = P_{rated} = constant\ . \tag{30}$$

Fig. 27 shows a family of these parameters as a function of rotor speed from 13.28 rpm to 18.26 rpm with a step of 0.83 rpm for a multi-MW wind turbine. The line with dots represents steady state operating conditions producing rated power, i.e. a set of parameters, (Ω_{ro}, v_o, β_o), at the rated rotor speed. The line with the highest pitch angle at wind speeds above 17 m/s corresponds to steady state operating conditions at a rotor speed of 13.28 rpm, and the line at the bottom is for 18.26 rpm. The relationship between a set of parameters, (Ω_{r0}, v_0, β_0), in Fig. 27 can be expressed as

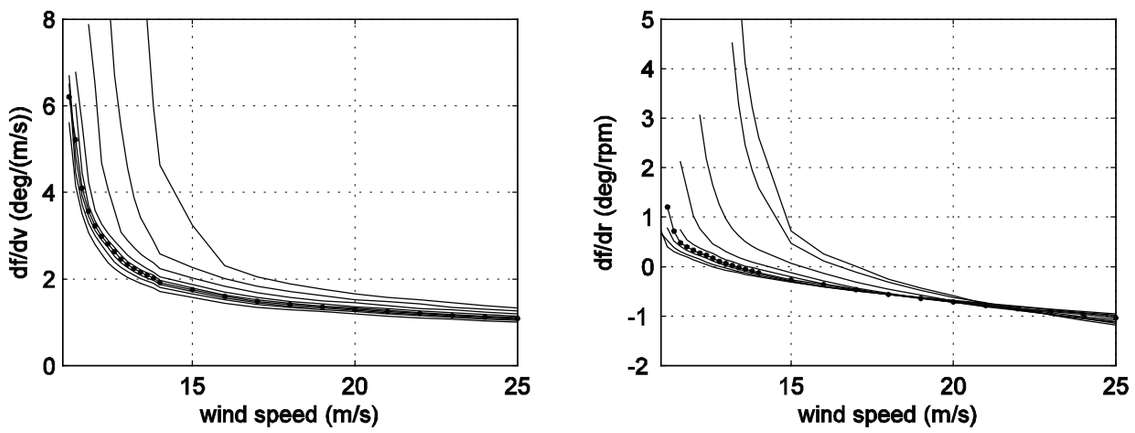

Fig. 28. A sample of $(\partial f/\partial v)_o$ and $(\partial f/\partial \Omega_r)_o$ as a function of wind speed and rotor rpm for a multi-MW wind turbine

$$\beta_0 = f(v_0, \Omega_{r_0}) \,. \tag{31}$$

The above equation means that the pitch angle should be maintained at β_0 for a wind speed of v_0 and a rotor speed of Ω_{r0} in order for a wind turbine to output a rated power. Assuming a sudden change of the wind speed from v_0 to $v_0+\delta v$ and the rotor speed from Ω_{r0} to $\Omega_{r0}+\delta\Omega_r$, the above equation can be approximated as

$$\begin{aligned} &\beta_0 + \delta\beta \simeq f(v_0, \Omega_{r_0}) + \left(\frac{\partial f}{\partial v}\right)_o \delta v + \left(\frac{\partial f}{\partial \Omega_r}\right)_o \delta\Omega_r \\ &\Rightarrow \quad \delta\beta = \left(\frac{\partial f}{\partial v}\right)_o \delta v + \left(\frac{\partial f}{\partial \Omega_r}\right)_o \delta\Omega_r \end{aligned} \,, \tag{32}$$

where $\delta\beta$ is the amount of pitch angle to compensate the combined variations of wind speed and rotor speed. This amount is $\delta\beta_{FF}$ in Fig. 25, which is the feedforward command to the pitch control system. Fig. 28 shows a sample of $(\partial f/\partial v)_o$ and $(\partial f/\partial \Omega_r)_o$ as a function of wind speed for several rotor speeds. The same set of rotor rpm as used in Fig. 27 is applied in this calculation. The line with dots in this figure represents the variation of $(\partial f/\partial v)_o$ and $(\partial f/\partial \Omega_r)_o$ with wind speed for the rated rotor speed. The lines at the top in both plots correspond to the variation of these gains for a rotor speed of 13.28 rpm. Note that the signs of $(\partial f/\partial v)_o$ and $(\partial f/\partial \Omega_r)_o$ at most wind speeds above rated are opposite. This results from the contrary aerodynamic effects of the wind and rotor speed on the rotating blades. An increase in the wind speed makes the angle of attack of the rotor blade larger, while an increase in the rotor speed makes it smaller (Manwell et al., 2009).

The simulation results for a 2 MW wind turbine using the above feedforward algorithm are summarized in Fig. 29. In this simulation, a torque schedule of the A-B-C-D-E-F shape in Fig. 10 is applied with the PI pitch controller. The first plot of this figure is the hub height wind speed, of which the mean and turbulence intensity are 16 m/s and 18%. The second is the estimated wind speed. The straight line in these plots represents the rated wind speed of the wind turbine, which is 11 m/s. The estimation was based on the Kalman filter of Eq. (29). In this calculation, 5% of the rated rpm and 8% of the rated torque are assumed as

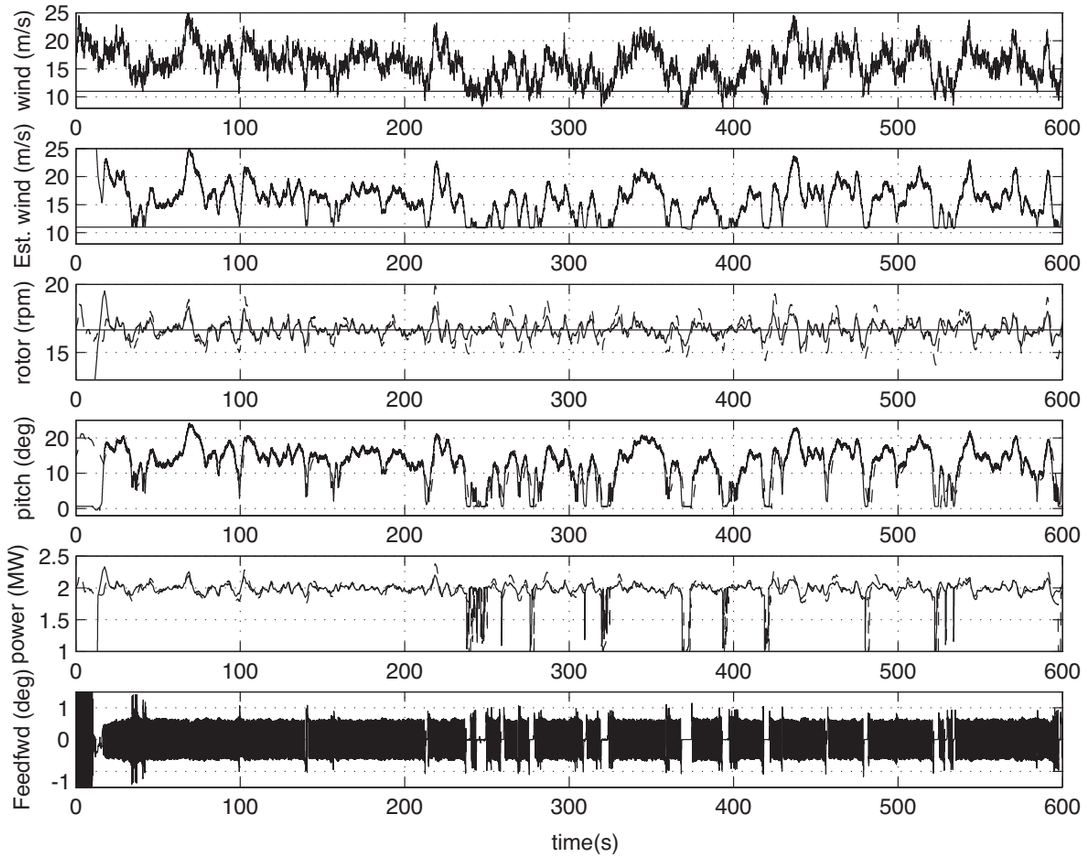

Fig. 29. Simulation results of the feedforward control for the mean wind speed of 16 m/s and 18% turbulence intensity

Performance data		Feedforward on	Feedforward off
Rotor speed (rpm)	Mean	16.6720	16.6408
	Standard deviation	0.4956	0.8971
Power (MW)	Mean	1.9920	1.9959
	Standard deviation	0.0619	0.1031

Table 4. Rotor speed and power data for the feedforward control on and off

measurement and process noise, respectively. The estimation errors up to around 20 seconds are due to the mismatched initial conditions in the estimator. The estimated wind speed tracks well and looks like a low-pass filtered wind speed because of the estimator dynamics. Note that there is a lower bound in the wind speed estimation, which is the rated wind speed. The third plot of Fig. 29 is the rotor rpm. The solid line shows the rotor speed response when the feedforward control is active, while the dashed line shows the response when it is off. As shown in this plot and summarized in Table 4, the benefit of applying the feedforward control is clear. The fourth plot is the pitch response. The solid line shows the response when the feedforwad control is active. A more high-frequency pitching action can be noticed in the response, compared to the pitch response when the feedforward is off (dashed

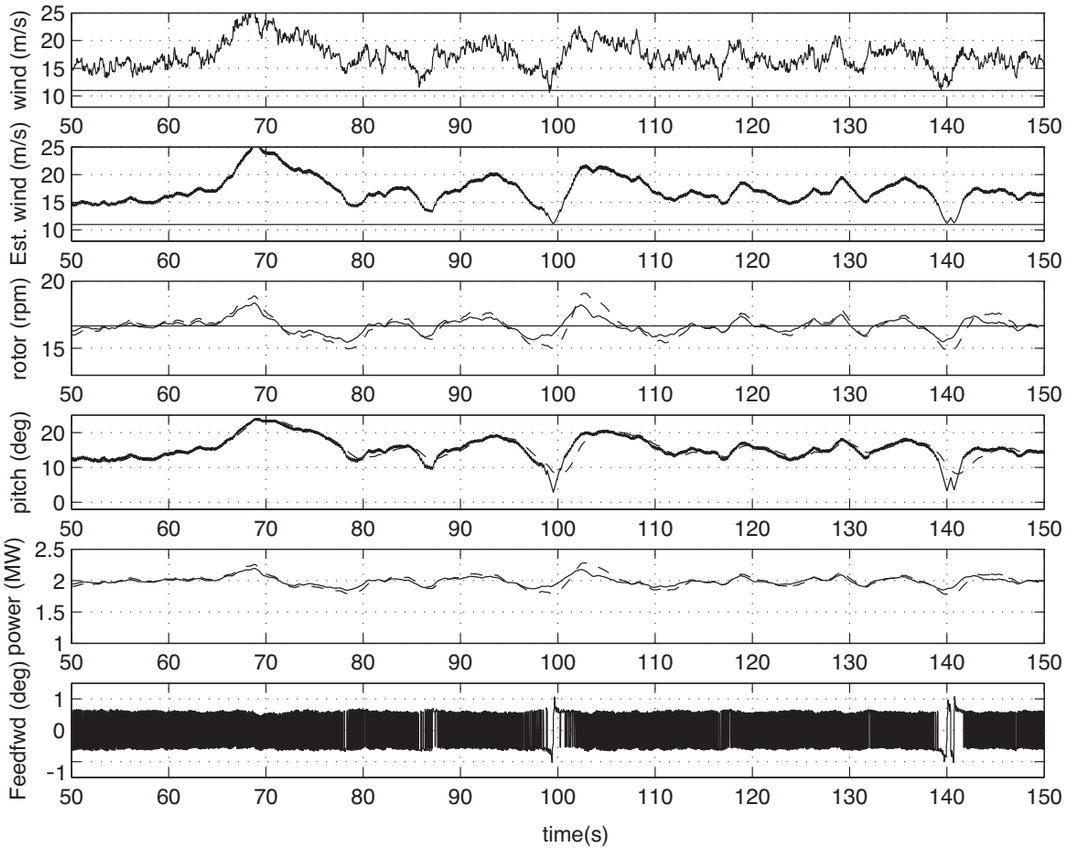

Fig. 30. Simulation results of the feedforward control for the time period from 50 to 150 seconds (re-plot of Fig. 29)

plot). Also note a time-ahead pitch motion in order to compensate the wind speed variation, compared to that of the baseline pitch control action, i.e. the pitch response when the feedforward is off. The fifth plot is the output power, which shows the performance of the feedforward control. Sudden drops of power in the response are due to the vertical torque schedule at the rated rpm (see the section E-F of Fig. 10). When the statistical data on power in Table 4 were calculated, the data during the power dip were not included. This is fair data processing, because the feedforward is not active for operating conditions in the below rated wind speed region. The final plot of this figure is the pitch demand by the feedforward control. Note that even where the magnitude of the pitch demand is not very large, there is distinct advantage in applying the feedforward control. The above mentioned points can also be seen in Fig. 30, which is a re-plot of Fig. 29 for a time period from 50 to 150 seconds.

4.4 Individual pitch control

The modern wind turbine is a huge mechanical structure. For example, the rotor diameter of even a 3 MW machine is over 90 m. In a turbulent wind condition, the wind speed variation of this machine experienced through a full rotation could easily be over 10 m/s, which imparts asymmetric aerodynamic forces to the rotating blades. During wind turbine operation, there are many sources of asymmetric forces on a blade such as

- vertical and horizontal wind shear

- turbulent winds
- yawing misalignment
- gravitational effect due to tilt angle, tower shadowing, etc.

These forces are periodic with rotational angle, i.e. azimuth angle except those due to turbulence. Theoretically, periodic forces can be reduced by cyclic pitch control using azimuth angle information. However, because of stochastic mechanical loadings by turbulent winds, it is not sufficient to cover the problem of load alleviation using only cyclic pitch control.

Prior to discussion of individual pitch control, we will define mechanical loads in two coordinate systems, namely the blade coordinate system and hub coordinate system of Fig. 31 (Bossanyi, 2009). The system on the right side of Fig. 31 is the blade coordinate system, which is attached to the blade. The ZB-axis is along the blade pitch axis, the XB-axis points towards the tower, and the YB-axis completes a right-handed coordinate system. The plane which is made by the ZB-axis during full rotational motion is the rotor in-plane. The rotor out-of-plane is clear from this definition. Note that the force and moment relation between the in-plane/out-of-plane and flapwise/edgewise direction at each blade section is given by

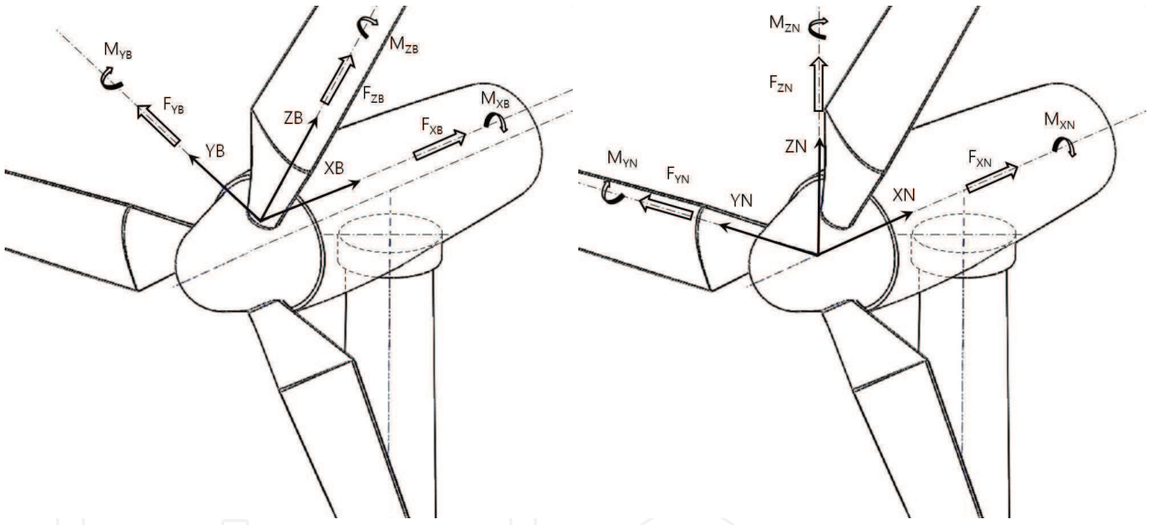

Fig. 31. Hub and blade coordinate system

$$\begin{Bmatrix} M_{XB} \\ M_{YB} \end{Bmatrix} = \begin{bmatrix} \sin(\theta_T + \beta) & \cos(\theta_T + \beta) \\ \cos(\theta_T + \beta) & -\sin(\theta_T + \beta) \end{bmatrix} \begin{Bmatrix} M_{FLAP} \\ M_{EDGE} \end{Bmatrix} \tag{33}$$

where θ_T and β represent the twist and pitch angle at the blade section, respectively. M_{XB} and M_{YB} are the bending moments at any blade section in the in-plane and out-of-plane direction, while M_{FLAP} and M_{EDGE} are the bending moments at the same blade section in the flapwise and edgewise direction. Note that strain gauge measurements on the blade root are usually made along the flapwise and edgewise directions.

The hub coordinate system is shown on the left side of Fig. 31 and is a fixed reference system. The XN-axis coincides with the shaft axis pointing towards the tower, the ZN-axis is in a vertically upward direction but inclined with a tilt angle, and the YN-axis completes a right-handed coordinate system. The out-of-plane bending moment of each blade at the root

section, i.e. M_{YB1}, M_{YB2}, M_{YB3}, can be transformed to a tilting moment, M_{YN}, and a yawing moment, M_{ZN}, in the hub coordinate system, that is

$$\begin{Bmatrix} M_{YN} \\ M_{ZN} \end{Bmatrix} = \begin{bmatrix} \cos\psi_1 & \cos\psi_2 & \cos\psi_3 \\ \sin\psi_1 & \sin\psi_2 & \sin\psi_3 \end{bmatrix} \begin{Bmatrix} M_{YB1} \\ M_{YB2} \\ M_{YB3} \end{Bmatrix} \tag{34}$$

where ψ_i is the azimuth angle of the i-th blade and is defined as zero when the blade is in the upright position. The above equation shows how the blade loads developed in a rotating reference frame are transferred to the tower in a fixed reference frame. The transform of Eq. (34) is similar to the inverse Coleman transform (van Engelen et al., 2007) or the d-q axis transform for electric machinery (Bossanyi, 2003; Krause et al., 2002), which is just a change of variables from a rotating to a fixed reference frame, that is

$$\begin{Bmatrix} M_{F1} \\ M_{F2} \\ M_{F3} \end{Bmatrix} = \begin{bmatrix} 1/3 & 1/3 & 1/3 \\ 2/3\cos\psi_1 & 2/3\cos\psi_2 & 2/3\cos\psi_3 \\ 2/3\sin\psi_1 & 2/3\sin\psi_2 & 2/3\sin\psi_3 \end{bmatrix} \begin{Bmatrix} M_{YB1} \\ M_{YB2} \\ M_{YB3} \end{Bmatrix} \tag{35}$$

where M_{F1}, M_{F2}, and M_{F3} are variables in a fixed reference frame. M_{F1} is the average of three variables M_{YB1}, M_{YB2}, M_{YB3}. Note that M_{F2} and M_{F3} are proportional to a tilting moment, M_{YN}, and a yawing moment, M_{ZN}, in the hub coordinate system. The inverse of the transform of Eq. (35) is the Coleman transform, which is given by

$$\begin{Bmatrix} M_{YB1} \\ M_{YB2} \\ M_{YB3} \end{Bmatrix} = \begin{bmatrix} 1 & \cos\psi_1 & \sin\psi_1 \\ 1 & \cos\psi_2 & \sin\psi_2 \\ 1 & \cos\psi_3 & \sin\psi_3 \end{bmatrix} \begin{Bmatrix} M_{F1} \\ M_{F2} \\ M_{F3} \end{Bmatrix}. \tag{36}$$

The above relation illuminates the core idea of the individual pitch control (IPC) algorithm. If M_{F2} and M_{F3} can be maintained close to zero, then only small amounts of oscillatory out-of-plane motion of the blade result. This is self-evident from Eq. (36). Fig. 32 is a block diagram representation of the above IPC algorithm. As shown in this figure, the first step of the IPC is to transform the bending moment of each blade in the out-of-plane direction to fixed frame quantities, i.e. M_{F2} and M_{F3}. The next step is the application of appropriate control laws which make M_{F2} and M_{F3} zero. The final step is to convert the amounts of pitch demand calculated in the fixed frame to quantities of individual pitch demand by using the Coleman transform.

A schematic structure of a wind turbine control system with the IPC algorithm is depicted in Fig. 33. As mentioned in the above, the core of the individual pitch control (IPC) is how to minimize the magnitudes of M_{F2} and M_{F3}. The same pitch and torque control structure as that explained in Section 2.2 (compare Fig. 33 with Fig. 7) is applied. Two control loops, i.e. the power curve tracking control loop (pitch and torque control loop) and the IPC loop, are not coupled, so the independent design of each loop is possible. Reduction of mechanical loads on the blades is a critical issue for a large wind turbine, because the amplitude of mechanical loads is directly related with the life cycle of the blades. The efficiency of the IPC algorithm depends on how the control laws are programmed. Various IPC control laws and simulation results can be found in the references (Selvam, 2007; Bossanyi & Wright, 2009; van Engelen, 2007).

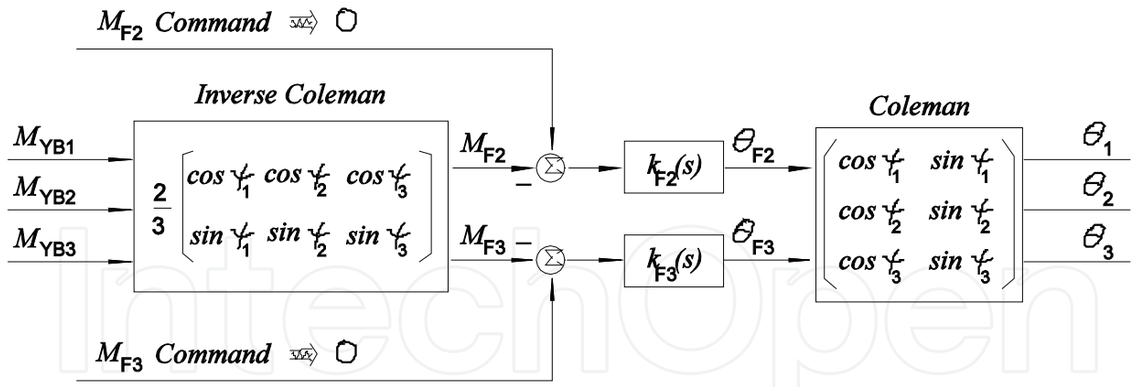

Fig. 32. Schematic of IPC algorithm

Because of the diverse sources of cyclic loads such as wind shear, tower shadowing, etc., most mechanical loads on blades consist of a 1p (1 per revolution, i.e. rotational frequency) component and its harmonics as shown in the upper part of Fig. 34. Due to averaging through a full rotation of the rotor, however, only the 3p and its harmonics of mechanical loads are left and transferred to the hub, drive train, and generator. Noting that the azimuth angle of the i-th blade can be represented as $\psi_i=\omega t+ \psi_{i0}$ in Eq. (36), where ω is the 1p in the unit of r/s, the relationship of the mechanical loads between a rotating reference frame and a fixed reference frame can be understood. As depicted in this figure, the 0p and 1p motions in a rotating frame affect only the 0p motion in a fixed frame. The IPC algorithm explained in Fig. 32 is based on the 1p motion control, which is effective only in decreasing the 1p component magnitude of the blade mechanical loads, in other words, DC mechanical loads in the non-rotating frame, such as the yaw bearing moments. In order to alleviate the 3p component of non-rotating mechanical loads, the 2p IPC should be applied. The 2p IPC has the same control structure as that of the 1p IPC in Fig. 32, but the arguments in sine and cosine functions should be doubled (Bossanyi & Wright, 2009).

The simulation results of applying the IPC algorithm to a 3 MW wind turbine are summarized in Fig. 35, Fig. 36, and Fig. 37. The IPC simulation was performed in the GH Bladed© (Bossanyi, 2008) environment. Simple proportional controllers for $k_{F2(s)}$ and $k_{F3(s)}$ are used in this IPC simulation. The wind speed shown in these figures is the hub height wind speed, which has a mean of 20 m/s and 10% turbulence intensity. Fig. 35 contains the performance-related time responses, which are the rotor speed (rpm), the #1 pitch angle (deg), the generator torque (kNm), and the power (MW). The dashed lines in these figures represent the time domain responses, which are obtained when the IPC is off. As expected, there is almost no interaction between the power curve tracking control and IPC loop. The dashed plot in the third window of Fig. 35 is the #1 pitch response when the IPC is off, while the solid plot is the response when it is on. The 1p pitching is dominant in the solid plot, which results from the IPC action to minimize the blade bending moment in the out-of-plane direction. The effect of the IPC on the blade load alleviation is shown in Fig. 36. The first window is the wind speed, which is the same wind as that in Fig. 35. The three consecutive plots after this are the bending moments of #1, #2, and #3 blade at the root section in the out-of-plane direction. Again, the dashed lines are the responses when the IPC is off. Note how the peak-to-peak magnitude of the out-of-plane bending moment of each blade is changed with the application of the IPC. As summarized in Table 5, there are more than 20% DEL decreases of the blade moments in the out-of-plane direction for all blades.

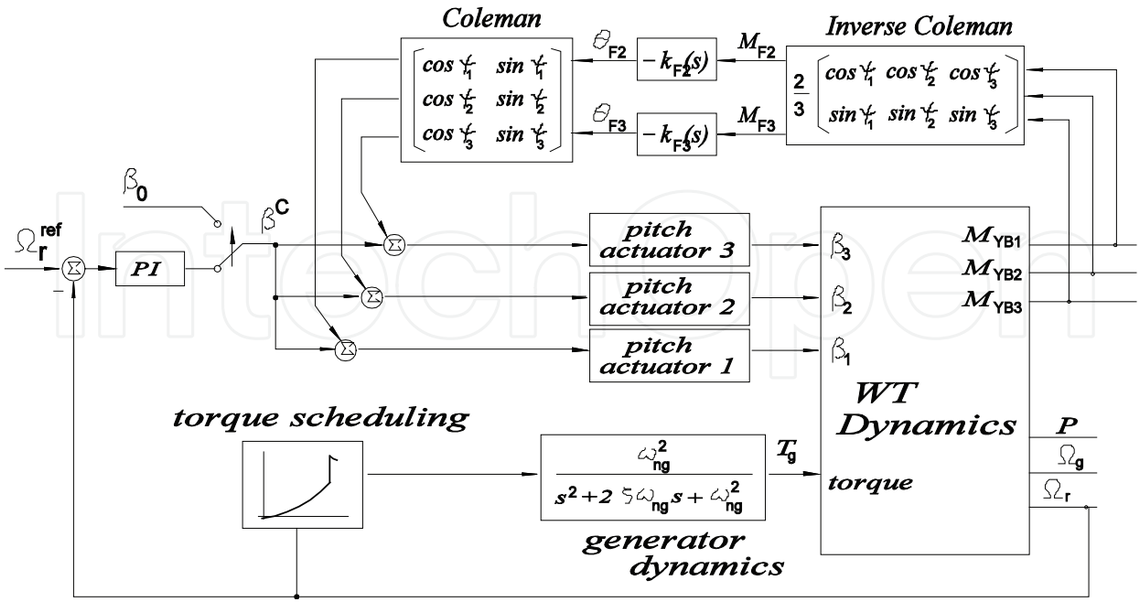

Fig. 33. Schematic of collective pitch control system with IPC algorithm

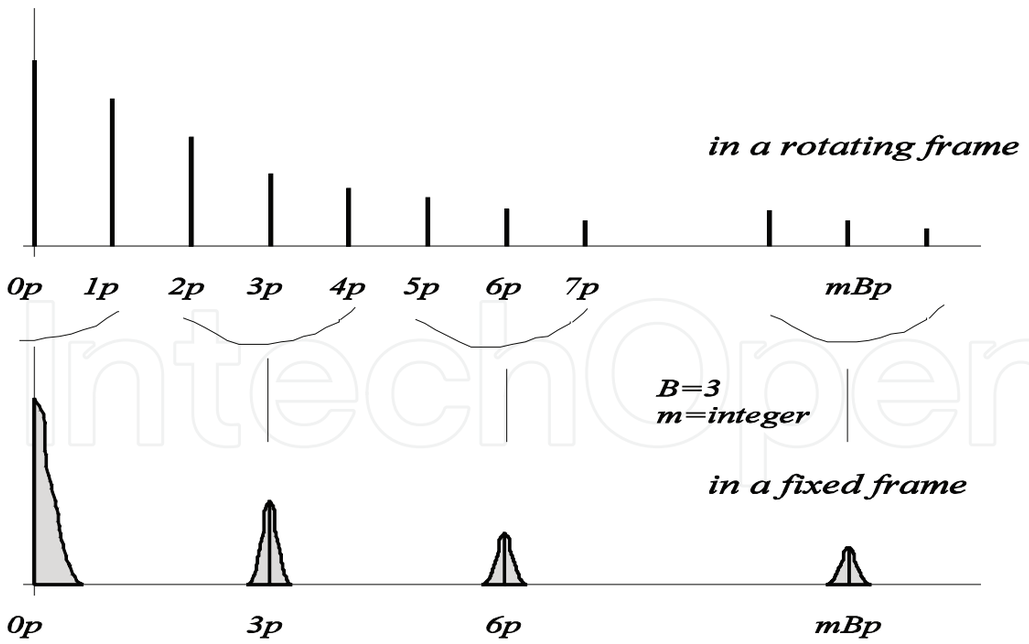

Fig. 34. Amplitudes of harmonic components for the mechanical loads in a rotating and fixed frame

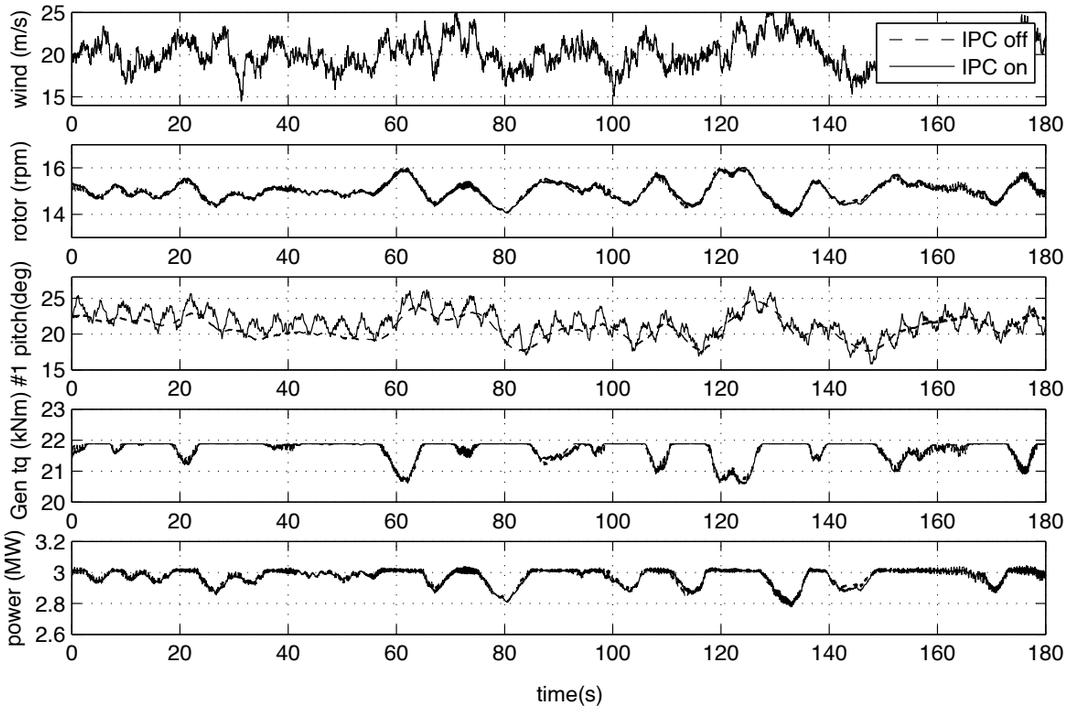

Fig. 35. Time domain responses of performance related data when the IPC is on (solid lines) and off (dashed lines)

The final three plots of Fig. 36 are M_{F1}, M_{F2}, and M_{F3}. Due to the averaging of three blade moments, M_{F1} comes to have the 3p component signal. Note how much the mean levels of M_{F2} and M_{F3} move toward zero when the IPC is on. As mentioned earlier, the core of the IPC algorithm is minimization of M_{F2} and M_{F3} (see Fig. 32). Depending on how $k_{F2(s)}$ and $k_{F3(s)}$ of Fig. 32 are designed, the performance of the IPC, i.e. how large the mean values of M_{F2} and M_{F3} are, would be determined. Even for the application of a simple proportional IPC controller, the above simulation results look promising. The tower root bending moments in the side-side and fore-aft direction are shown in the second and third windows of Fig. 37. The peak-to-peak magnitudes of the tower mechanical loads are increased when the IPC is on. Especially, the tower loads in the side-side direction deteriorate more than those in the fore-aft (see Table 5). The fourth window of Fig. 37 is the yawing moment of the yaw bearing. Note the similarity between this plot and the M_{F3} response of Fig. 36. The final three plots of Fig. 37 are the blade pitch angles of all three blades. The dashed line shows the collective pitch response when the IPC is off.

5. Conclusions

Control system design of wind turbines is a complex task which has to consider the various aspects of performance and safety issues of wind turbine operation. The role of the control system becomes more critical in a multi-MW wind turbine design. This chapter covers all the areas of control system design. Starting from a simple drive train model, how a PI pitch controller is designed and what are the critical design problems are explained. Some interesting themes of wind speed estimation, feedforward pitch control, and individual pitch control system design are included, together with numeric simulation results.

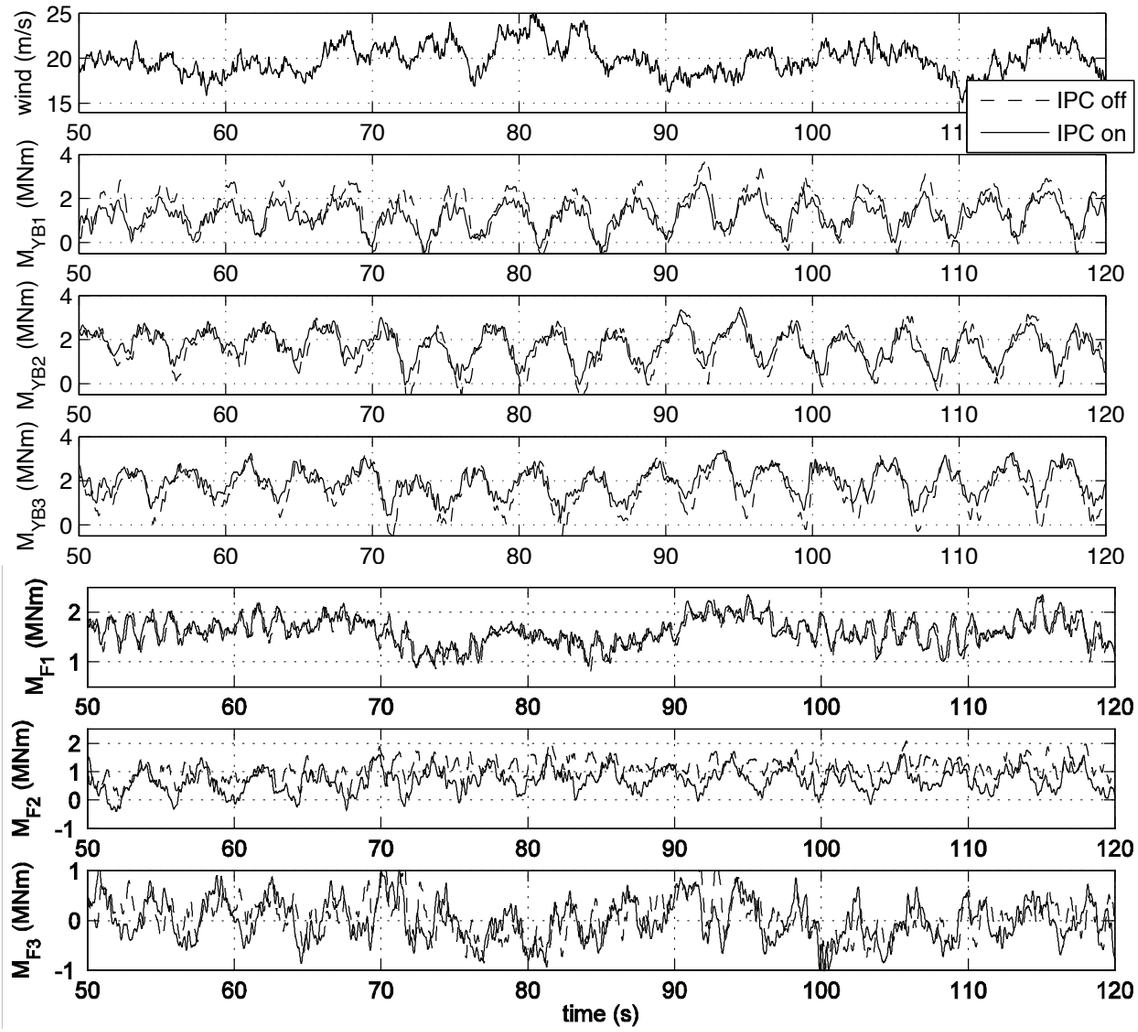

Fig. 36. Time domain responses of blade mechanical loads when the IPC is on (solid lines) and off (dashed lines)

	Blade loads in the out-of-plane direction (MNm)			Tower loads (MNm)	
	#1 blade	#2 blade	#3 blade	Side-side	Fore-aft
IPC off (A)	2.906	2.906	2.906	9.212	12.66
IPC on (B)	2.097	2.275	2.184	11.32	13.14
(B-A)/A (%)	-27.87	-21.71	-24.84	22.8	3.79

Table 5. Damage equivalent loads (DEL) of out-of-plane blade bending moments and tower root moments with IPC on and off

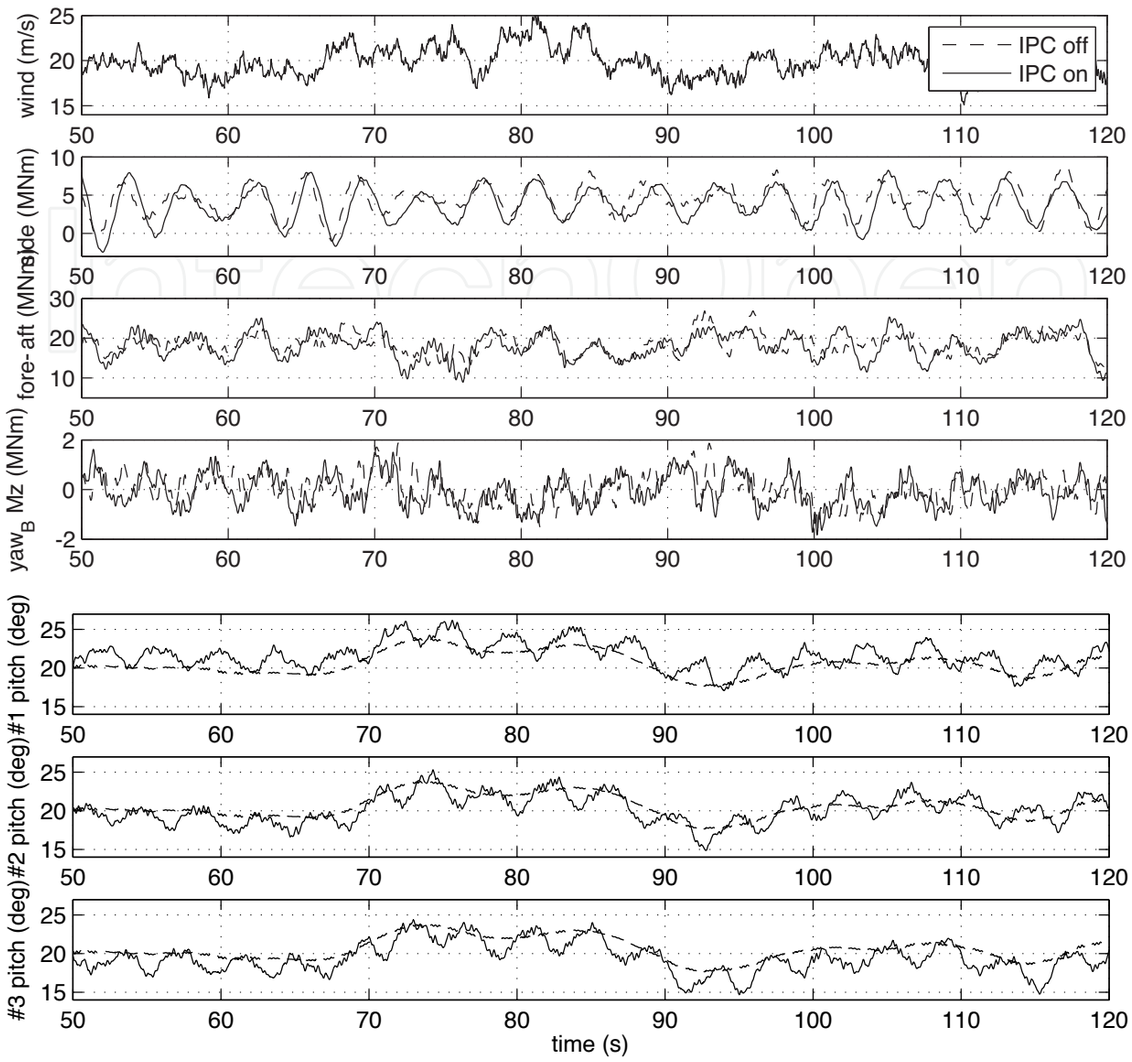

Fig. 37. Time domain responses of tower loads, yaw bearing loads, and blade pitches when the IPC is on (solid lines) and off (dashed lines)

6. References

Bianchi, F.; Battisa, H. & Mantz, R. (2007). Wind turbine control systems, principles, modelling and gain scheduling design, Springer, ISBN: 1846284929

Bossanyi, E. (2009). GH Bladed user manual (version 3.81), Garrad Hassan and Partners, 282-BR-010

Bossanyi, E. (2008). GH Bladed theory manual (version 3.81), Garrad Hassan and Partners, 282-BR-009

Bossanyi, E. & Wright, A. (2009). Field testing of individual pitch control on the NREL CART-2 wind turbine, EWEC2009-European Wind Energy Conference & Exhibition

Bossanyi, E. (2003). Individual blade pitch control for load reduction. Wind Energy, No. 6, pp. 119-128, ISSN: 1099-1824

Bossanyi, E. (2000). The design of closed loop controllers for wind turbines. Wind Energy, No. 3, pp. 149-163, ISSN: 1099-1824

Boukhezzar, B.; Lupu, L., Siguerdidjane, H. & Hand, M. (2007). Multivariable control strategy for variable speed variable pitch wind turbines. Renewable Energy, Vol. 32, pp. 1273-1287, ISSN: 0960-1481

Burton, T.; Sharpe, D., Jenkins, N. & Bossanyi, E. (2001). Wind energy handbook, A John Wiley and Sons, ISBN: 9780471489979

Dominguez, S. & Leithead, W. (2006). Size related performance limitations on wind turbine control performance, International Control Conference (ICC 2006), FB4-181, Glasgow

Dorf, R. & Bishop, R. (2007). Modern control systems, Prentice Hall, ISBN: 0132270285.

Franklin, G.; Powell, J. & Emami-Naeini, A. (2006). Feedback control of dynamic system, Prentice Hall, ISBN: 0-13-149930-0

Gelb, A. (1974). Applied optimal estimation, The MIT Press, ISBN: 10- 0262570483

Haque, M.; Negnevitsky, M. & Muttaqi, K. (2010). A novel control strategy for a variable-speed wind turbine with a permanent-magnet synchronous generator. IEEE Transactions on Industry Applications, Vol. 46, Issue 1, pp. 331-339, ISSN: 0093-9994

Krause, P.; Wasynczuk, O. & Sudhoff, S. (2002). Analysis of electric machinery and drive systems, A John Wiley and Sons, ISBN: 0-471-14326-X

Leithead[a], W. & Connor, B. (2000). Control of variable speed wind turbines: dynamic models. International Journal of Control, Vol. 73, No. 13, pp. 1173-1188, ISSN: 0020-7179

Leithead[b], W. & Connor, B. (2000). Control of variable speed wind turbines: design task. International Journal of Control, Vol. 73, No. 13, pp. 1189-1212, ISSN: 0020-7179

Leloudas, G.; Zhu, W. Sorensen, J., Shen, W. & Hjort, S. (2007). Prediction and reduction of noise for a 2.3MW wind turbine. Journal of Physics: Conference series, Vol. 75, pp. 1-9, ISSN: 1742-6588

Manwell, J.; McGowan, J. & Rogers, A. (2009). Wind energy explained, Theory, design and application, A John Wiley and Sons, ISBN: 9780470015001

Muller, S.; Deicke, M. & de Donker, R. (2002). Doubly fed induction generator systems for wind turbines. IEEE Industry Applications Magazine, May-June 2002, pp. 26-33, ISSN: 1077-2618

Ostergaard, K; Brath, P. & Stoustrup, J. (2007). Estimation of effective wind speed. Journal of Physics: Conference series, Vol. 75, pp. 1-9, doi: 10.1088/1742-596/75/1 /012082

Selvam, I. (2007). Individual pitch control for large scale wind turbines, ECN-E-07-053

Soter, S. & Wegerer, R. (2007). Development of induction machines in wind power technology, IEMDC 2007-IEEE International Electrical Machines and Drives Conference, pp. 1490-1495

van Engelen, T. (2007). Control design based on aero-hydro-servo-elastic linear models fromTURBU(ECN), ECN-M-07-054

van Engelen, T.; Markou, H., Buhl, T. & Marrant, B. (2007). Morphological study of aeroelastic control for wind turbines, ECN-E-06-056

van der Hooft, E.; Schaak, P., & van Engelen, T. (2003). Wind turbine control algorithm, ECN-C-03-111

van der Hooft, E. & van Engelen, T. (2003). Feedforward control of estimated wind speed, ECN-C-03-137

van der Hoven (1957). Power spectrum of horizontal wind speed spectrum in the frequency range from 0.0007 to 900 cycles per hour. Journal of Meteorology, Vol. 14, pp. 160-164

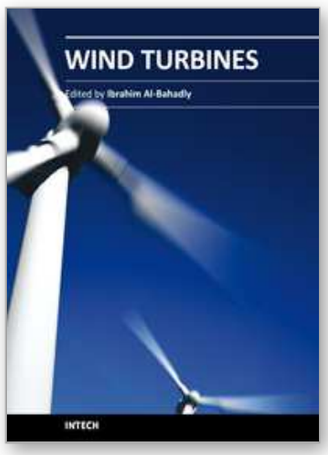

Wind Turbines

Edited by Dr. Ibrahim Al-Bahadly

ISBN 978-953-307-221-0
Hard cover, 652 pages
Publisher InTech
Published online 04, April, 2011
Published in print edition April, 2011

The area of wind energy is a rapidly evolving field and an intensive research and development has taken place in the last few years. Therefore, this book aims to provide an up-to-date comprehensive overview of the current status in the field to the research community. The research works presented in this book are divided into three main groups. The first group deals with the different types and design of the wind mills aiming for efficient, reliable and cost effective solutions. The second group deals with works tackling the use of different types of generators for wind energy. The third group is focusing on improvement in the area of control. Each chapter of the book offers detailed information on the related area of its research with the main objectives of the works carried out as well as providing a comprehensive list of references which should provide a rich platform of research to the field.

INTECH
open science | open minds

InTech Europe
University Campus STeP Ri
Slavka Krautzeka 83/A
51000 Rijeka, Croatia
Phone: +385 (51) 770 447
Fax: +385 (51) 686 166
www.intechopen.com

InTech China
Unit 405, Office Block, Hotel Equatorial Shanghai
No.65, Yan An Road (West), Shanghai, 200040, China
中国上海市延安西路65号上海国际贵都大饭店办公楼405单元
Phone: +86-21-62489820
Fax: +86-21-62489821

IntechOpen